Research Article **Open Access**

Sulian Thual* and Andrew J. Majda

A Suite of Skeleton Models for the MJO with Refined Vertical Structure

DOI 10.1515/mcwf-2015-0004
Received August 6, 2015; accepted October 27, 2015

Abstract: The Madden-Julian oscillation (MJO) is the dominant mode of variability in the tropical atmosphere on intraseasonal timescales and planetary spatial scales. The skeleton model is a minimal dynamical model that recovers robustly the most fundamental MJO features of (I) a slow eastward speed of roughly 5 ms^{-1}, (II) a peculiar dispersion relation with $d\omega/dk \approx 0$, and (III) a horizontal quadrupole vortex structure. This model depicts the MJO as a neutrally-stable atmospheric wave that involves a simple multiscale interaction between planetary dry dynamics, planetary lower-tropospheric moisture and the planetary envelope of synoptic-scale activity.

Here we propose and analyze a suite of skeleton models that qualitatively reproduce the refined vertical structure of the MJO in nature. This vertical structure consists of a planetary envelope of convective activity transitioning from the congestus to the deep to the stratiform type, in addition to a front-to-rear (i.e. tilted) structure of heating, moisture, winds and temperature. A first example of skeleton model achieving this goal has been considered recently in work by the authors. The construction of such a model satisfies an energy conservation principle, such that its solutions at the intraseasonal-planetary scale remain neutrally stable. Here, additional classes of skeleton models are constructed based on the same principle. In particular, those new models are more realistic then the former one as they consider fully coupled interactions between the planetary dry dynamics of the first and second baroclinic mode and the details of the vertical structure of moisture and convective activity. All models reproduce qualitatively the refined vertical structure of the MJO. In addition, when considered with a simple stochastic parametrization for the unresolved details of synoptic-scale activity, all models show intermittent initiation, propagation and shut down of MJO wave trains, as in previous studies.

1 Introduction

The dominant component of intraseasonal variability in the tropics is the 40 to 50 day intraseasonal oscillation, often called the Madden-Julian oscillation (MJO) after its discoverers [22, 23]. In the troposphere, the MJO is an equatorial planetary-scale wave, that is most active over the Indian and western Pacific Oceans and propagates eastward at a speed of around 5 ms^{-1}. The planetary-scale circulation anomalies associated with the MJO significantly affect monsoon development, intraseasonal predictability in midlatitudes, and the development of El Niño events in the Pacific Ocean.

In addition to the above features, the MJO in nature propagates eastward with an interesting vertical structure. Observations reveal a central role of three cloud types above the boundary layer in the MJO: lower-middle troposhere congestus cloud decks that moisten and precondition the lower troposphere in the initial phase, followed by deep convection and a trailing wake of upper troposphere stratiform clouds. Observa-

***Corresponding Author: Sulian Thual:** Department of Mathematics, and Center for Atmosphere Ocean Science, Courant Institute of Mathematical Sciences, New York University, 251 Mercer Street, New York, NY 10012 USA, E-mail: sulian.thual@gmail.com
Andrew J. Majda: Department of Mathematics, and Center for Atmosphere Ocean Science, Courant Institute of Mathematical Sciences, New York University, 251 Mercer Street, New York, NY 10012 USA

tions also reveal that the MJO envelope consists of a complex front-to-rear (i.e. tilted) vertical structure as seen on all main dynamical fields such as heating, winds, temperature, and moisture [18, 19, 42]. There is an ongoing effort to evaluate comprehensively the vertical structure of the MJO simulated by global weather and climate models [11, 20, 44]. In addition, significant progress as been made for describing the vertical structure of various convective events at synoptic scale and mesoscale that are part of the convective envelope of the MJO [28, 32]. Khouider and Majda [13–15] developed a systematic multicloud model convective parametrization highlighting the nonlinear dynamical role of the three cloud types, congestus, stratiform, and deep convective clouds, and their different heating vertical structures. The multicloud model reproduces key features of the observational record for mesoscale and synoptic-scale convectively coupled waves, as well as a realistic MJO envelope analog for an intraseasonal parameter regime [25]. The multicloud model has also been used as a cumulus parametrization in GCM experiments with consequent improvement of the simulated MJO variability [1, 6, 17]. As another example, the role of synoptic scale waves in producing key features of the MJO's vertical structure has been elucidated in multiscale asymptotic models [2, 3, 24, 37], with focus for example on the role of convective momentum transport [26, 30].

While theory and simulation of the MJO remain difficult challenges, they are guided by some generally accepted, fundamental features of the MJO on intraseasonal-planetary scales that have been identified relatively clearly in observations [10, 43, 45]. These features, referred to here as the MJO's "skeleton" features, are (I) a slow eastward phase speed of roughly 5 ms^{-1}, (II) a peculiar dispersion relation with $d\omega/dk \approx 0$, and (III) a horizontal quadrupole structure. Majda and Stechmann [27] introduced a minimal dynamical model, the skeleton model, that captures the MJO's intraseasonal features (I-III) together for the first time in a simple model. The model is a coupled nonlinear oscillator model for the MJO skeleton features as well as tropical intraseasonal variability in general. In particular, there is no instability mechanism at planetary scale, and the interaction with sub-planetary convective processes discussed above is accounted for, at least in a crude fashion. In a collection of numerical experiments, the non-linear skeleton model has been shown to simulate realistic MJO events with significant variations in occurrence and strength, asymmetric east-west structures, as well as a preferred localization over the background state warm pool region [28]. A stochastic version of the skeleton model has also been developed that includes a simple stochastic parametrization of the unresolved synoptic-scale convective/wave processes [40, 41]. In addition to the above features (I-III), this model reproduces additional realistic features such as the intermittent generation of MJO events and the organization of MJO events into wave trains with growth and demise [29, 36]. The skeleton model has also been shown to reproduce realistic solutions for a realistic background state of heating/moistening [34], to provide an essential theoretical estimate of the intensity of MJO events in observations [38], and has been used recently for twin-experiment forecasts [4, 5].

In recent work [39], the authors have proposed and analyzed a skeleton model that reproduces qualitatively, for the first time, the front-to-rear vertical structure of the MJO found in nature. This includes MJO events marked by a planetary envelope of convective activity transitioning from the congestus to the deep to the stratiform type, in addition to a front-to-rear structure of heating, moisture, winds and temperature. This goal is achieved by introducing new variables in the original skeleton model [27] that include additional details of the vertical structure, such as a detailed separation of convective activity into congestus, deep and stratiform activity [13], a separation of overall moisture into lower and middle level moisture, as well as the dry dynamics of both the first and second baroclinic mode. Here, we introduce and analyze additional classes of skeleton models that also achieve this goal. The models are designed following similar major design principles, such as the conservation of a positive energy and a moist static energy. As compared to the skeleton model with refined vertical structure from [39], the models proposed here have richer dynamics. For instance the additional circulation that grasps more details of the vertical structure is here fully coupled to the dynamical core of the skeleton model (instead of forced by it).

The article is organized as follows. In section 2 we recall the design and main features of the original skeleton model and we introduce the new classes of skeleton models with refined vertical structure used here. See most particularly section 2.6 where the main features of each of those models are summarized and contrasted. In sections 3, 5 and 4 we show solutions for each new class of skeleton model. Section 6 is a discussion with concluding remarks. In appendix A we briefly show the solutions of a simple skeleton model

with refined vertical structure used for illustration in section 2, and in appendix B we analyze briefly a single-column model version of the model from section 3.

2 A Suite of Skeleton Models with Refined Vertical Structure

2.1 Nonlinear Skeleton Model

The skeleton model has been proposed originally by Majda and Stechmann [27] (hereafter MS2009), and further analyzed in Majda and Stechmann [28] (hereafter MS2011) and Thual, Majda and Stechmann [41] (hereafter TMS2014). It is a minimal non-linear oscillator model for the MJO and the intraseasonal-planetary variability in general. The design of the skeleton model, already presented in those previous publications, is recalled here briefly for completeness.

The fundamental assumption in the skeleton model is that the MJO involves a simple multiscale interaction between (i) planetary-scale dry dynamics, (ii) lower-level moisture q and (iii) the planetary-scale envelope of synoptic-scale convective/wave deep activity, a. The planetary envelope a in particular is a collective (i.e. integrated) representation of the convective/wave activity occurring at sub-planetary scale (i.e. at synoptic-scale and possibly at mesoscale), the details of which are unresolved. It is assumed that environment moisture influences the tendency (i.e. the growth and decay rates) of the envelope of convective activity:

$$\partial_t a = \Gamma q a \,, \tag{1}$$

where $\Gamma > 0$ is a constant of proportionality: positive (negative) low-level moisture anomalies create a tendency to enhance (decrease) the envelope of convective activity.

In the skeleton model, the $q - a$ interaction parametrized in Eq. (1) is further combined with the linear primitive equations projected on the first vertical baroclinic mode. This reads, in non-dimensional units,

$$\begin{aligned}
&\partial_t u_1 - y v_1 - \partial_x \theta_1 = 0 \\
&y u_1 - \partial_y \theta_1 = 0 \\
&\partial_t \theta_1 - (\partial_x u_1 + \partial_y v_1) = \overline{H} a - s_1^\theta \\
&\partial_t q + \overline{Q}(\partial_x u_1 + \partial_y v_1) = -\overline{H} a + s^q \\
&\partial_t a = \Gamma q a \,,
\end{aligned} \tag{2}$$

with periodic boundary conditions along the equatorial belt. The first three rows of Eq. (2) describe the dry atmosphere dynamics, with equatorial long-wave scaling as allowed at planetary scale. The u_n, v_n, θ_n are the zonal, meridional velocity, and potential temperature anomalies, respectively, for the baroclinic mode $n = 1$. The fourth row describes the evolution of low-level moisture q. The fifth row is the above Eq. (1). All variables are anomalies from a radiative-convective equilibrium (RCE), except a. This model contains a minimal number of parameters: $\overline{Q}$ is the background vertical moisture gradient, Γ is a proportionality constant. The $\overline{H}$ is irrelevant to the dynamics (as can be seen by rescaling a) but allows to define a heating/drying rate $\overline{H}a$ for the system in dimensional units. The s_1^θ and s^q are external sources of cooling and moistening, respectively, that need to be prescribed in the system (see hereafter).

An important peculiarity of the skeleton model is that there is no instability mechanism at planetary scale, with a tacit assumption that the primary instabilities and damping occur on synoptic scales (MS2009). For instance, for a RCE with balanced external sources of cooling/moistening, $\overline{H}\overline{a} = s_1^\theta = s^q$, the system in Eq. (2) conserves a total positive energy (as there are no dissipative processes):

$$\partial_t [\frac{1}{2} u_1^2 + \frac{1}{2} \theta_1^2 + \frac{1}{2} \frac{\overline{Q}}{1 - \overline{Q}} (\theta_1 + \frac{q}{\overline{Q}})^2 + \frac{\overline{H}}{\overline{Q}\Gamma} (a - \overline{a} log(a))] - \partial_x (u_1 \theta_1) - \partial_y (v_1 \theta_1) = 0 \,, \tag{3}$$

For this reason, the linear solutions of the skeleton model are neutrally-stable (i.e with no growth/decay over time). In addition to this, the skeleton model conserves a vertically integrated moist static energy:

$$\partial_t (\theta_1 + q) - (1 - \overline{Q})(\partial_x u_1 + \partial_y v_1) = 0 \,. \tag{4}$$

The skeleton model depicts the MJO as a neutrally-stable planetary wave. For instance, the linear solutions of the system of Eq. (2) (truncated meridionally) exhibit a MJO mode with essential observed features, namely a slow eastward phase speed of roughly 5 ms^{-1}, a peculiar dispersion relation with $d\omega/dk \approx 0$ and a horizontal quadrupole structure (MS2009; MS2011, see also hereafter).

2.2 Guiding Principles

In this section we detail the guiding principles that are considered to derive new classes of skeleton model with refined vertical structure. In order to illustrate those guiding principles, we will derive in this section one of the simplest skeleton model with refined structure, that consists of the original skeleton model presented above with an additional coupling to middle level moisture.

The main motivation for the new classes of skeleton models is to add variables to the original skeleton model from Eq. (2) in order to reproduce qualitatively the front-to-rear vertical structure of the MJO found in nature. This front-to-rear vertical structure is observed on many variables such as heating, moisture, winds, temperature, etc (e.g. [19]). Here for simplicity assume that we want to account for the front-to-rear structure of moisture. For this, we introduce middle tropospheric moisture anomalies q_m as a new variable: we expect in particular q_m anomalies (at middle level) to trail behind q anomalies (at lower level) in the simulated MJO envelope, resulting in a tilted structure of moisture by construction. The original skeleton model from Eq. (2) is extended with coupling to this new variable. This reads, in non-dimensional units:

$$\begin{aligned}
&\partial_t u_1 - y v_1 - \partial_x \theta_1 = 0 \\
&y u_1 - \partial_y \theta_1 = 0 \\
&\partial_t \theta_1 - (\partial_x u_1 + \partial_y v_1) = \overline{H} a - s_1^\theta \\
&\partial_t q_m = F_l (q + \overline{Q}\theta_1) \\
&\partial_t q + \overline{Q}(\partial_x u_1 + \partial_y v_1) = -\overline{H} a + s^q - F_m q_m \\
&\partial_t a = \Gamma q a
\end{aligned} \tag{5}$$

with new parameters F_l and F_m that parametrize moisture flux exchanges from the lower to the middle troposphere.

The above model from Eq. (5) satisfies an energy conservation principle, such that its solutions at the intraseasonal-planetary scale remain neutrally stable as in the original skeleton model (MS2009). The total positive energy from Eq. (3) is now rewritten as:

$$\partial_t [\frac{1}{2}u_1^2 + \frac{1}{2}\theta_1^2 + \frac{1}{2}\frac{\overline{Q}}{1-\overline{Q}}(\theta_1 + \frac{q}{\overline{Q}})^2 + \frac{\overline{H}}{\overline{Q}\Gamma}(a - \overline{a}log(a)) + \frac{1}{2}\frac{1}{(1-\overline{Q})\overline{Q}}\frac{F_m}{F_l}q_m^2] - \partial_x(u_1\theta_1) - \partial_y(v_1\theta_1) = 0 \tag{6}$$

with the inclusion of a new term associated to middle-level moisture. This energy conservation principle shapes the form of the skeleton model from Eq. (5), with in particular a moisture flux term proportional to $(q + \overline{Q}\theta_1)$ in the middle troposphere (as can be shown by cancelling quadratic terms in the energy budget). Another desirable feature when constructing new models is the conservation of a moist static energy, as in Eq. (4). The above model however does not have this feature. For instance its moist static energy budget reads:

$$\partial_t(\theta_1 + q + q_m) - (1 - \overline{Q})(\partial_x u_1 + \partial_y v_1) = F_l(q + \overline{Q}\theta_1) - F_m q_m \tag{7}$$

with a non-zero r.h.s due to the moisture flux exchange terms. Finally, a detailed analysis of the model solutions is necessary afterwards in order to verify that the model reproduces a MJO with realistic front-to-rear structure (here on moisture), in addition to conserving important features of the original skeleton model (see e.g. features I-III in the introduction of this article). For this, we will analyze here linear solutions as well as solutions from numerical experiments with a stochastic parametrization for the synoptic activity (see hereafter).

The above building principles are considered to design the new classes of skeleton models with refined vertical structure presented hereafter. Those models consider several new variables in order to account for

the front-to-rear structure of the MJO on fields such as heating, winds, temperature, etc. The model with coupling to middle level moisture from Eq. (5) is rather simple in comparison and so its solutions are only briefly presented in the appendix section A of this article.

2.3 Model with Three Convective Activities

In recent work, Thual and Majda [39], (hereafter TM2015) have proposed and analyzed a skeleton model that reproduces qualititatively, for the first time, the front-to-rear vertical structure of MJO events found in nature. This model is constructed based on the above building principles, and is presented here for completeness.

The original skeleton model from Eq. (2) depicts MJO dynamics associated to an envelope of overall convective activity a, with a coarse vertical structure (MS2009, MS2011). In order to produce MJO events with refined vertical structure, several envelopes of convective activity have been considered in TM2015, namely congestus activity a_c, deep activity a_d and stratiform activity a_s. This reads, in non-dimensional units,

$$\begin{aligned}
&\partial_t u_1 - y v_1 - \partial_x \theta_1 = 0 \\
&y u_1 - \partial_y \theta_1 = 0 \\
&\partial_t \theta_1 - (\partial_x u_1 + \partial_y v_1) = \overline{H}(\xi_{1d} a_d + \xi_{1s} a_c + \xi_{1c} a_s) - s_1^\theta \\
&\partial_t q + \overline{Q}(\partial_x u_1 + \partial_y v_1) = -\overline{H}(\xi_{1d} a_d + \xi_{1c} a_c + \xi_{1c} a_s) + s^q \\
&\partial_t a_c = \Gamma_c(\xi_{1c} q + \beta_s r_s - \beta_c r_d)(a_c - \epsilon_c r_c) \\
&\partial_t a_d = \Gamma_d(\xi_{1d} q + \beta_c r_c - \beta_d r_s)(a_d - \epsilon_d r_d) \\
&\partial_t a_s = \Gamma_s(\xi_{1s} q + \beta_d r_d - \beta_s r_c)(a_s - \epsilon_s r_s)
\end{aligned} \tag{8}$$

where $r_d = a_d - \overline{a}_d$, $r_c = a_c - \overline{a}_c$ and $r_s = a_s - \overline{a}_s$ are convective activity anomalies to the radiative-convective equilibrium (RCE) state. The Γ_c, Γ_d, Γ_s are growth rates, β_c, β_d, β_s are transition rates between each type of convective activity, ϵ_c, ϵ_d, ϵ_s are pseudo-dissipation coefficients that limit the exponential growth of convective activity, and ξ_{1c}, ξ_{1d} and ξ_{1s} are projection coefficients (see TM2015 and hereafter). All parameters are positive and $0 \leq \epsilon_c, \epsilon_d, \epsilon_s \leq 1$. Note that each convective activity heats and dries the atmosphere at the same time. For consistency with previous work on the skeleton model, deep activity a_d that is usually most prominent in the MJO envelope may be considered as most representative of overall convective activity a. Therefore, for $a_d = a$, $\xi_{1d} = 1$, $\epsilon_d = 0$ and $a_c, a_s = 0$ we retrieve the original skeleton model from Eq. (2).

The relationships in Eq (8) are chosen based on several criteria. First, they are consistent with the relatonships of the original skeleton model as well as with empirical relationships between different convective activites found elsewhere (e.g. in the multicloud model, see [12, 13]). Second, they conserve a total positive energy for a RCE with balanced external sources ($s_1^\theta = s^q$), an important requisite for the skeleton model to exhibit neutral solutions. The energy budget reads (see Eq. 3 for comparison):

$$\begin{aligned}
&\partial_t [E_1 + E_c + E_d + E_s] + A_1 = 0 \\
&E_1 = (\overline{Q}/\overline{H})[\tfrac{1}{2} u_1^2 + \tfrac{1}{2} \theta_1^2 + \tfrac{1}{2} (\overline{Q}(1-\overline{Q}))^{-1} (q_1 + \overline{Q}\theta_1)^2] \\
&A_1 = (\overline{Q}/\overline{H})[-\partial_x (u_1 \theta_1) - \partial_y (v_1 \theta_1)] \\
&E_c = \Gamma_c^{-1} (1-\epsilon_c)^{-2} (a_c - \epsilon_c a_c - \overline{a}_c \log(a_c)) \\
&E_d = \Gamma_d^{-1} (1-\epsilon_d)^{-2} (a_d - \epsilon_d a_d - \overline{a}_d \log(a_d)) \\
&E_s = \Gamma_s^{-1} (1-\epsilon_s)^{-2} (a_s - \epsilon_s a_s - \overline{a}_s \log(a_s)) \,.
\end{aligned} \tag{9}$$

The model also conserves a vertically integrated moist static energy (identical to the one of the original skeleton model, see Eq. 4):

$$\partial_t (\theta_1 + q) - (1 - \overline{Q})(\partial_x u_1 + \partial_y v_1) = 0 \,. \tag{10}$$

In addition to the dynamical core of the skeleton model from Eq. (8), we consider a slaved secondary circulation. This secondary circulation does not feed back on to the dynamical core of the model, which is

somewhat unrealistic, but allows nevertheless to grasp in a simple fashion more details of the vertical structure. The secondary circulation reads, in non-dimensional units:

$$\begin{aligned}
&\partial_t u_2 - y v_2 - \partial_x \theta_2/2 = 0\\
&y u_2 - \partial_y \theta_2/2 = 0\\
&\partial_t \theta_2 - (\partial_x u_2 + \partial_y v_2)/2 = \overline{\overline{H}}(\xi_{2c} a_c - \xi_{2s} a_s) - s_2^\theta\\
&\partial_t q_m = M(a_c - a_s) + s_m^q\\
&\partial_t q_l + \overline{Q}(\partial_x u_1 + \partial_y v_1) = -\overline{\overline{H}}(\xi_d a_d + \xi_c a_c + \xi_c a_s) - \alpha M(a_c - a_s) + s_l^q
\end{aligned} \tag{11}$$

where u_n, v_n, θ_n are the zonal, meridional velocity, and potential temperature anomalies, respectively, for the baroclinic mode $n = 2$. The s_2^θ is an external source of cooling and ξ_{2c}, ξ_{2s} are projection coefficients (see hereafter). We assume here that q is a vertically integrated estimate of moisture that decomposes into $q = q_l + \alpha q_m$, where q_l is moisture anomalies at bottom level and q_m at middle level (see TM2015). In addition to the main drying and moisture convergence occuring at lower level, congestus and stratiform activity favors moisture exchange between the lower and middle level at a rate M (e.g. through detrainment or downdrafts, see [13]). Noteworthy, the above equations sum up to the moisture budget of $q = q_l + \alpha q_m$ in Eq. (8) for external sources of moistening satisfying $s^q = s_l^q + \alpha s_m^q$.

2.4 Model with Coupled Potential Temperature

Following the building principles proposed in the above sections, we propose here another class of skeleton model with coupling to potential temperature. One drawback of the skeleton model with three convective activities (see Eq. 8) is the presence of a secondary slaved circulation (see Eq. 12), which is somewhat unrealistic. In order to avoid this feature, the strategy consists here in allowing convective activity to grow/decay depending on potential temperature. As a result, the dry dynamics of the second baroclinic mode dynamics are now fully coupled to the dynamical core of the model. The model reads, in non-dimensional units:

$$\begin{aligned}
&\partial_t u_n - y v_n - \partial_x \theta_n/n = 0\\
&y u_n - \partial_y \theta_n/n = 0\\
&\partial_t \theta_1 - (\partial_x u_1 + \partial_y v_1) = \overline{\overline{H}}(\xi_{1d} a_d + \xi_{1c} a_c + \xi_{1s} a_s) - s_1^\theta\\
&\partial_t \theta_2 - (\partial_x u_2 + \partial_y v_2)/2 = \overline{\overline{H}}(\xi_{2c} a_c - \xi_{2s} a_s) - s_2^\theta\\
&\partial_t q + \overline{Q}(\partial_x u_1 + \partial_y v_1) + \lambda\overline{Q}(\partial_x u_2 + \partial_y v_2)/2 = -\overline{\overline{H}}(\xi_{1c} a_c + \xi_{1d} a_d + \xi_{1s} a_s) + \lambda\overline{\overline{H}}(\xi_{2s} a_s - \xi_{2c} a_c) + s^q\\
&\partial_t a_c = \Gamma_c[\,(\xi_{1c} + \lambda\xi_{2c})q + (\lambda\xi_{2c}\overline{Q})\theta_1 + (\lambda\xi_{1c}\overline{Q})\theta_2 + \beta_s r_s - \beta_c r_d\,](a_c - \epsilon_c r_c)\\
&\partial_t a_d = \Gamma_d[\,\xi_{1d} q + (\lambda\xi_{1d}\overline{Q})\theta_2 + \beta_c r_c - \beta_d r_s\,](a_d - \epsilon_d r_d)\\
&\partial_t a_s = \Gamma_s[\,(\xi_{1s} - \lambda\xi_{2s})q - (\lambda\xi_{2s}\overline{Q})\theta_1 + (\lambda\xi_{1s}\overline{Q})\theta_2 + \beta_d r_d - \beta_s r_c\,](a_s - \epsilon_s r_s)
\end{aligned} \tag{12}$$

As compared to the skeleton model from TM2015 (obtained for $\lambda = 0$, see Eq. 8 for comparison), the moisture budget for q here further includes moisture convergence due to the second baroclinic mode and drying/moistening due to congestus and stratiform activity, with a parameter $\lambda \geq 0$ in factor of both terms. In the r.h.s of the moisture budget, $-\overline{\overline{H}}(\xi_{1c} a_c + \xi_{1d} a_d + \xi_{1s} a_s)$ roughly corresponds to drying by first baroclinic mode deep convection (precipitation), while $\lambda\overline{\overline{H}}(\xi_{2s} a_s - \xi_{2c} a_c)$ roughly corresponds to moistening by second baroclinic mode downdrafts (see e.g. [13]). The details of lower and middle level moisture (q_l and q_m where $q = q_l + \alpha q_m$) are here omitted though they could easily be included into a secondary slaved circulation (e.g. as in TM2015). The growth/decay of convective activities in Eq. (12) is similar to the one of the model from TM2015, except for a dependency on potential temperature $\lambda\theta_1$ and $\lambda\theta_2$. For instance $\lambda\theta_1 \geq 0$ favors the growth of congestus activity a_c and the decay of stratiform activity a_s, while $\lambda\theta_2 \geq 0$ favors the growth of all convective activities. This peculiar dependency on potential temperature allows the model from Eq. (12) to

conserve a total positive energy for a RCE with balanced external sources ($s_1^\theta + \lambda s_2^\theta = s^q$). This reads:

$$\begin{aligned}
&\partial_t[E_1 + E_2 + E_Z + E_c + E_d + E_s] + A_1 + A_2 = 0\\
&E_1 = (\overline{Q}/\overline{H})[\tfrac{1}{2}u_1^2 + \tfrac{1}{2}\theta_1^2]\\
&E_2 = (\lambda^2\overline{Q}/\overline{H})[\tfrac{1}{2}u_2^2 + \tfrac{1}{2}\theta_2^2]\\
&A_1 = (\overline{Q}/\overline{H})[-\partial_x(u_1\theta_1) - \partial_y(v_1\theta_1)]\\
&A_2 = (\lambda^2\overline{Q}/\overline{H})[-\partial_x(u_2\theta_2)/2 - \partial_y(v_2\theta_2)/2]\\
&E_Z = (\overline{H}(1-\overline{Q}))^{-1}[\tfrac{1}{2}Z^2]\\
&E_c = \Gamma_c{}^{-1}(1-\epsilon_c)^{-2}(a_c - \epsilon_c a_c - \overline{a}_c\log(a_c))\\
&E_d = \Gamma_d{}^{-1}(1-\epsilon_d)^{-2}(a_d - \epsilon_d a_d - \overline{a}_d\log(a_d))\\
&E_s = \Gamma_s{}^{-1}(1-\epsilon_s)^{-2}(a_s - \epsilon_s a_s - \overline{a}_s\log(a_s))
\end{aligned} \tag{13}$$

where $Z = q + \overline{Q}\theta_1 + \lambda\overline{Q}\theta_2$. This results from the balance of terms:

$$\begin{aligned}
&\partial_t E_1 + A_1 = (\xi_{1c}r_c + \xi_{1d}r_d + \xi_{1s}r_s)\overline{Q}\theta_1\\
&\partial_t E_2 + A_2 = (\xi_{2c}r_c - \xi_{2s}r_s)\lambda^2\overline{Q}\theta_2\\
&\partial_t E_z = -(q + \overline{Q}\theta_1 + \lambda\overline{Q}\theta_2)[(\xi_{1c} + \lambda\xi_{2c})r_c + \xi_{1d}r_d + (\xi_{1s} - \lambda\xi_{2s})r_s]\\
&\partial_t E_c = [(\xi_{1c} + \lambda\xi_{2c})q + (\lambda\xi_{2c}\overline{Q})\theta_1 + (\lambda\xi_{1c}\overline{Q})\theta_2 + \beta_s r_s - \beta_c r_d]r_c\\
&\partial_t E_d = [\xi_{1d}q + (\lambda\xi_{1d}\overline{Q})\theta_2 + \beta_c r_c - \beta_d r_s]r_d\\
&\partial_t E_s = [(\xi_{1s} - \lambda\xi_{2s})q - (\lambda\xi_{2s}\overline{Q})\theta_1 + (\lambda\xi_{1s}\overline{Q})\theta_2 + \beta_d r_d - \beta_s r_c]r_s
\end{aligned} \tag{14}$$

In addition to this, the model conserves a vertically integrated moist static energy, with contribution from both the first and second baroclinic mode:

$$\partial_t(q + \theta_1 + \lambda\theta_2) - (1-\overline{Q})(\partial_x u_1 + \partial_y v_1) - \lambda(1-\overline{Q})(\partial_x u_2 + \partial_y v_2)/2 = 0 \tag{15}$$

2.5 Model with Coupled Lower and Middle Tropospheric Moisture

We propose here another class of skeleton model with coupling to the details of lower and middle tropospheric moisture. In order to avoid the presence of a secondary slaved circulation as in the skeleton model with three convective activities from Eq. (8), the strategy consists here in allowing convective activity to grow/decay depending on both lower and middle tropospheric moisture, instead of potential temperature as in section 2.4. The model reads, in non-dimensional units:

$$\begin{aligned}
&\partial_t u_n - y v_n - \partial_x\theta_n/n = 0\\
&y u_n - \partial_y\theta_n/n = 0\\
&\partial_t\theta_1 - (\partial_x u_1 + \partial_y v_1) = \overline{H}(\xi_{1d}a_d + \xi_{1c}a_c + \xi_{1s}a_s) - s_1^\theta\\
&\partial_t\theta_2 - (\partial_x u_2 + \partial_y v_2)/2 = \overline{H}(\xi_{2c}a_c - \xi_{2s}a_s) - s_2^\theta\\
&\partial_t q_1 + \overline{Q}_1(\partial_x u_1 + \partial_y v_1) = -\overline{H}(\xi_{1d}a_d + \xi_{1c}a_c + \xi_{1s}a_s) - s_1^q\\
&\partial_t q_2 + \overline{Q}_2(\partial_x u_2 + \partial_y v_2)/2 = -\overline{H}(\xi_{2c}a_c - \xi_{2s}a_s) - s_2^q\\
&\partial_t a_c = \Gamma_c(\alpha_1\xi_{1c}q_1 + \alpha_2\xi_{2c}q_2 + \beta_s r_s - \beta_c r_d)(a_c - \epsilon_c r_c)\\
&\partial_t a_d = \Gamma_d(\alpha_1\xi_{1d}q_1 + \beta_c r_c - \beta_d r_s)(a_d - \epsilon_d r_d)\\
&\partial_t a_s = \Gamma_s(\alpha_1\xi_{1s}q_1 - \alpha_2\xi_{2s}q_2 + \beta_d r_d - \beta_s r_c)(a_s - \epsilon r_s)
\end{aligned} \tag{16}$$

As in the skeleton model from TM2015 (obtained for $\alpha_1 = 1$ and $\alpha_2 = 0$, see Eq. 8 for comparison), $q = q_l + \alpha q_m$ is a vertically integrated estimate of moisture, and we introduce here $q_2 = q_l - \alpha q_m$ a measure of moisture vertical difference. The q_1 and q_2 are mathematically akin to a Galerkin projection (see e.g. [33]), for which drying and moisture convergence is controlled by either the first or second baroclinic mode, respectively. We assume in particular that second baroclinic mode convergence as well as congestus and stratiform activity can increase/decrease moisture vertical difference (due to their sign inversion at middle level). $\overline{Q}_2$ and s_2^q are moisture convergence and external moistening associated to the second baroclinic mode, respectively. The growth/decay of convective activities is identical to the one of the model from TM2015, but here in addition

positive moisture difference $q_2 \geq 0$ favors the growth of congestus activity a_c and the decay of stratiform activity a_s. This peculiar dependency on moisture allows the model from Eq. (16) to conserve a total positive energy for a RCE with balanced external sources ($s_1^\theta = s_l^q$, $s_2^\theta = s_m^q$). This reads:

$$\begin{aligned}
&\partial_t[\alpha_1 E_1 + \alpha_2 E_2 + E_c + E_d + E_s] + \alpha_1 A_1 + \alpha_2 A_2 = 0\\
&E_1 = (\overline{Q}_1/\overline{H})[\tfrac{1}{2}u_1^2 + \tfrac{1}{2}\theta_1^2 + \tfrac{1}{2}(\overline{Q}_1(1-\overline{Q}_1))^{-1}(q_1 + \overline{Q}_1\theta_1)^2]\\
&E_2 = (\overline{Q}_2/\overline{H})[\tfrac{1}{2}u_2^2 + \tfrac{1}{2}\theta_2^2 + \tfrac{1}{2}(\overline{Q}_2(1-\overline{Q}_2))^{-1}(q_2 + \overline{Q}_2\theta_2)^2]\\
&A_1 = (\overline{Q}_1/\overline{H})[-\partial_x(u_1\theta_1) - \partial_y(v_1\theta_1)]\\
&A_2 = (\overline{Q}_2/\overline{H})[-\partial_x(u_2\theta_2)/2 - \partial_y(v_2\theta_2)/2]\\
&E_c = \Gamma_c{}^{-1}(1-\epsilon_c)^{-2}(a_c - \epsilon_c a_c - \overline{a}_c\log(a_c))\\
&E_d = \Gamma_d{}^{-1}(1-\epsilon_d)^{-2}(a_d - \epsilon_d a_d - \overline{a}_d\log(a_d))\\
&E_s = \Gamma_s{}^{-1}(1-\epsilon_s)^{-2}(a_s - \epsilon_s a_s - \overline{a}_s\log(a_s))\,.
\end{aligned} \tag{17}$$

which is in essence the energy budget from Eq. (9) with additional contributions E_2 and A_2. In addition to this, the model conserves a vertically integrated moist static energy, with contribution from both the first and second baroclinic mode:

$$\partial_t(\theta_1 + \theta_2 + q_1 + q_2) - (1-\overline{Q}_1)(\partial_x u_1 + \partial_y v_1) - (1-\overline{Q}_2)(\partial_x u_2 + \partial_y v_2)/2 = 0\,. \tag{18}$$

2.6 Model Intercomparison

In this section we highlight and contrast the main features of each of the above models. Solutions for each model are presented in the next sections. Table 1 summarizes the main features of all models in addition to the original skeleton model (MS2009).

First, the main feature of the new skeleton models is that, as compared to the original skeleton model, they reproduce qualitatively the front-to-rear vertical structure of the MJO (see Fig. 3, 11, 7). Despite this interesting additional feature, all new models conserve a positive energy in addition to a moist static energy, as in the original skeleton model (see previous sections). The conservation of a total positive energy in particular is an important building principles ensuring that the intraseasonal-planetary dynamics remain neutrally stable (MS2009).

Second, the new models introduce several new variables, with for example a detailed separation of convective activity a into congestus activity a_c, deep activity a_d and stratiform activity a_s [13], a separation of overall moisture q into lower and middle level moisture q_l and q_m, and the dry dynamics of the second baroclinic mode, u_2, v_2, θ_2. All those new variables allow to grasp more details of the front-to-rear vertical structure of the MJO as compared to the coarse vertical structure from the original skeleton model (MS2009). The models strongly differ with respect to the separation of the dynamics into a coupled circulation and a secondary slaved circulation. In particular, the new models with coupled potential temperature or coupled lower and middle level moistures are fully coupled i.e. have no secondary slaved circulation, which is more realistic. A drawback of this higher dimensionality is the introduction in those models of several additional linear solutions, for example a slow eastward and westward mode, a zonally symmetric mode, etc (see e.g. Fig 2).

Finally, we analyze hereafter the solutions of each model with a stochastic parametrization for the synoptic-convective activity: most models show a prominent MJO variability, with however varying results (see Fig 5, 12, 8). The model with coupled lower and middle level moisture for example shows a MJO variability that is less prominent in comparison. In this model and the other ones to a lesser extent, a decrease in MJO variability can be due to the introduction of additional linear solutions that become as prominent as the MJO itself, notably because there are no dissipative processes. Hopefully the additional linear solutions are usually of a seasonal or interannual frequency and are therefore separable from the intraseasonal MJO variability. In addition all models simulate a consistent MJO variability, organized into intermittent wave trains with growth and demise (see Fig 6, 14, 10).

Table 1: Highlight and intercomparison of main model features.

Model	Original Skeleton (MS2009; MS2011; TMS2014)	Three convective activities (TM2015)	Coupled Potential Temperature	Coupled Lower and Middle level moisture
Section	2.1	2.3 and 3	2.5 and 4	2.5 and 5
MJO front-to-rear structure	no	yes	yes	yes
Conserved Positive Energy	yes	yes	yes	yes
Conserved Moist Static Energy	yes	yes	yes	yes
Coupled Circulation	u_1, v_1, θ_1, q, a	$u_1, v_1, \theta_1, q, a_d, a_c, a_s$	$u_1, v_1, \theta_1, u_2, v_2, \theta_2, q, a_d, a_c, a_s$	$u_1, v_1, \theta_1, u_2, v_2, \theta_2, q_l, q_m, a_d, a_c, a_s$
Secondary Slaved Circulation	none	$u_2, v_2, \theta_2, q_l, q_m$	none	none
Additional linear modes	none	Slow eastward Slow westward	Slow eastward Slow westward Dry Kelvin $n = 2$ Dry Rossby $n = 2$	Slow eastward Slow westward Zonally symmetric Dry Kelvin $n = 2$ Dry Rossby $n = 2$
Prominent MJO variability	yes	yes	yes	no

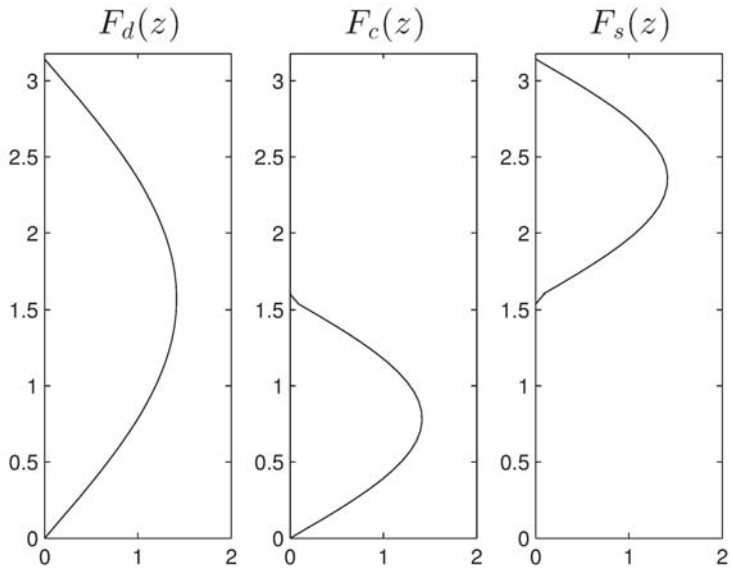

Figure 1: Vertical Structures $F_d(z)$, $F_c(z)$ and $F_s(z)$, as a function of z ($0 \le z \le \pi$ from the bottom to the tropopause).

2.7 Technical Details

We provide here some details on the vertical and meridional structure, stochastic parametrization and solving method, that are identical for each of the above skeleton models, as well as parameter values used to illustrate the solutions of each model.

The reconstructed fields for the skeleton models presented in the previous sections read $\{u, v\}(x, y, z, t) = \sum_n \{u_n, v_n\} F_n(z)$ and $\theta(x, y, z, t) = \sum_n \{\theta_n, s_n\} G_n(z)$, for $n = 1, 2$, with $F_n(z) = \sqrt{2}\cos(nz)$ and $G_n(z) = \sqrt{2}\sin(nz)$, for $0 \le z \le \pi$. The total convective activity reconstructs as $a(x, y, z, t) = a_c F_c(z) + a_d F_d(z) + a_s F_s(z)$, and is always positive. The vertical structures $F_d(z)$, $F_c(z)$ and $F_s(z)$ are shown in Fig. 1. We consider half-sinusoids $F_d = G_1$, $F_c = G_2$ for $0 \le z \le \pi/2$ and $F_s = -G_2$ for $\pi/2 \le z \le \pi$, as in [16]. The a_d, a_c and a_s are convective activity associated to the structures $F_d(z)$, $F_c(z)$ and $F_s(z)$. In most models we consider the dynamics of the first and second baroclinic modes, and therefore introduce the projection coefficients of convective activity on the first baroclinic mode, ξ_{1d}, ξ_{1c} and ξ_{1s}, and on the second baroclinic mode, ξ_{2c}, ξ_{2d} and ξ_{2s}. The projection coefficients have values $\xi_{1d} = 1$, $\xi_{1c}, \xi_{1s} = 4/3\pi\ \xi_{2c}, \xi_{2s} = 1/2$ (and $\xi_{2d} = 0$). Note that $\xi_{1d} \ge \xi_{1c}, \xi_{1s}$ therefore a unit of deep activity heats/dries the first baroclinic mode more than a unit of congestus or stratiform activity. Different values of those projection coefficients could however be considered assuming a more complex localization of heating/drying by convective activity, for example a decreased ξ_{1s} and increased ξ_{2s} due to radiative effects, etc (see [16] for a discussion).

To obtain the solutions in their simplest form, it is useful to further truncate each skeleton model to the first meridional structures (MS2009). For this we consider the parabolic cylinder functions:

$$\phi_{nm}(y) = \sqrt{\frac{\sqrt{n}}{2^m m! \sqrt{\pi}}} H_m(\sqrt{n}y) \exp(-ny^2/2) \tag{19}$$

for the baroclinic mode $n \ge 1$ and meridional mode $m \ge 0$, along with the Hermite polynomials $H_0(y) = 1$, $H_1(y) = 2y$, $H_2(y) = 4y^2 - 2$. We assume that all convective activities, moisture and external sources have a meridional profile ϕ_{10}, e.g. $\{a_c, a_s, a_d, q, s_1^\theta, s_2^\theta\} = \{A_c, A_s, A_d, Q, S_1^\theta, S_2^\theta\}\phi_{10}$, etc. A suitable change of variables is to introduce K_n and R_n, which are the amplitudes of the equatorial Kelvin wave and of the first Rossby wave for the baroclinic mode n, respectively. For instance, the meridional structure ϕ_{10} only excites K_1 and R_1 for $n = 1$, and for simplicity we assume that it only excites K_2 and R_2 for $n = 2$. The evolution of

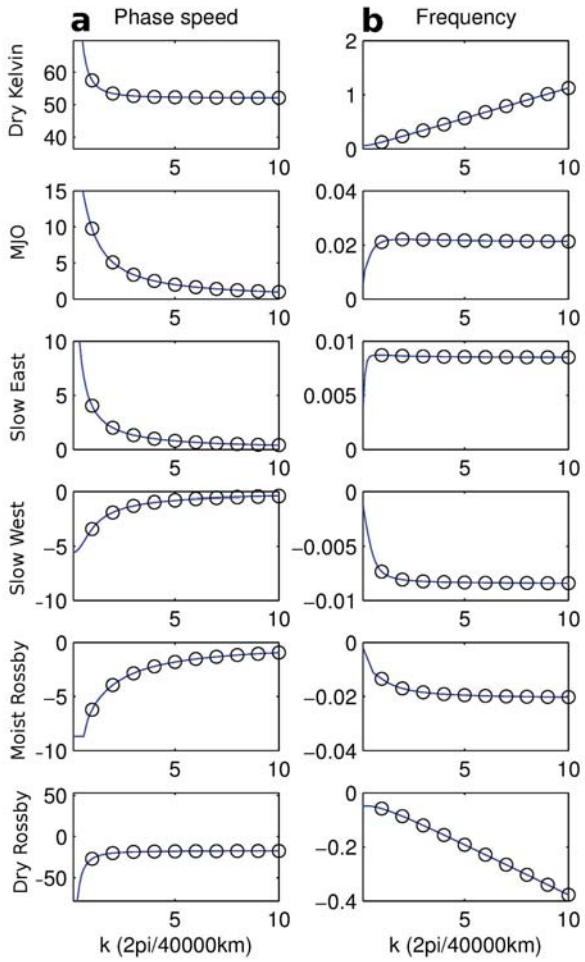

Figure 2: Skeleton model with three convective activities, summary of linear stability: (a) phase speed ω/k ($m.s^{-1}$), and (b) frequency ω (cpd), as a function of the zonal wavenumber k ($2\pi/40000$ km). The black circles mark the integer wavenumbers satisfying periodic boundary conditions. This is repeated for each eigenmode, from top to bottom in order of decreasing phase speed.

the Kelvin and Rossby wave amplitudes reads:

$$\begin{aligned} &\partial_t K_n + \partial_x K_n/n = -S_{n0} \\ &\partial_t R_n - \partial_x R_n/3n = -(4/3)S_{n0}\,, \end{aligned} \tag{20}$$

for $n = 1, 2$, where $S_{10} = \overline{H}(\xi_{1c}A_c + \xi_{1d}A_d + \xi_{1s}A_s) - S_1^\theta$ and where we approximate $S_{20} \approx \overline{H}(\xi_{2c}A_c - \xi_{2s}A_s) - S_2^\theta$. The variables of the dry dynamics component can be reconstructed using:

$$\begin{aligned} u_n &= (K_n/2 - R_n/4)\phi_{n0} + (R_n/4\sqrt{2})\phi_{n2} \\ v_n &= (\partial_x R_n - nS_{n0})(3\sqrt{2n})^{-1}\phi_{n1} \\ \theta_n &= -(K_n/2 + R_n/4)\phi_{n0} - (R_n/4\sqrt{2})\phi_{n2}\,. \end{aligned} \tag{21}$$

A stochastic version of each skeleton model is designed using a formalism similar to the one of TMS2014. The amplitude equations are replaced by stochastic birth/death processes (the simplest continuous-time Markov process, see chapter 7 of [8, 21]). This accounts for the irregular and intermittent contribution of unresolved synoptic activity to the intraseasonal-planetary dynamics. Let a_d be a random variable taking discrete values $a_d = \Delta a\, \eta_d$, where η_d is a non-negative integer. The probabilities of transiting from one state η_d to

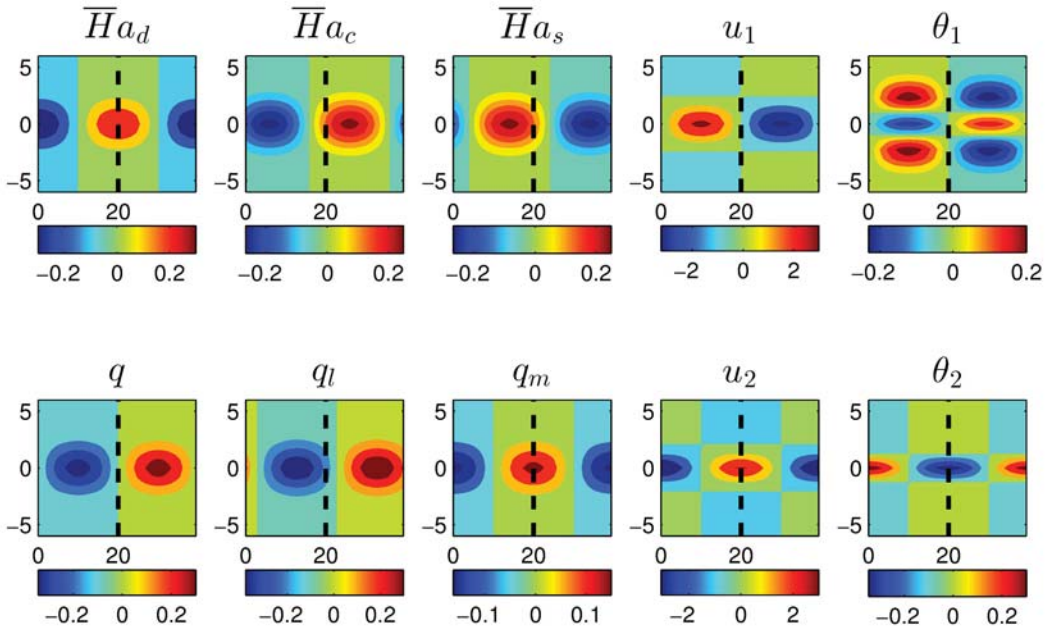

Figure 3: Skeleton model with three convective activities, structure $x - y$ of the MJO mode for $k = 1$, in dimensional units: $\overline{H}a_d$, $\overline{H}a_c$ and $\overline{H}a_s$ (Kday^{-1}), u_1(ms^{-1}), θ_1(K), q, q_l and q_m (K), u_2 (ms^{-1}), θ_2 (K), as a function of x and y (1000 km). The dashed line marks $x = 20,000$ km.

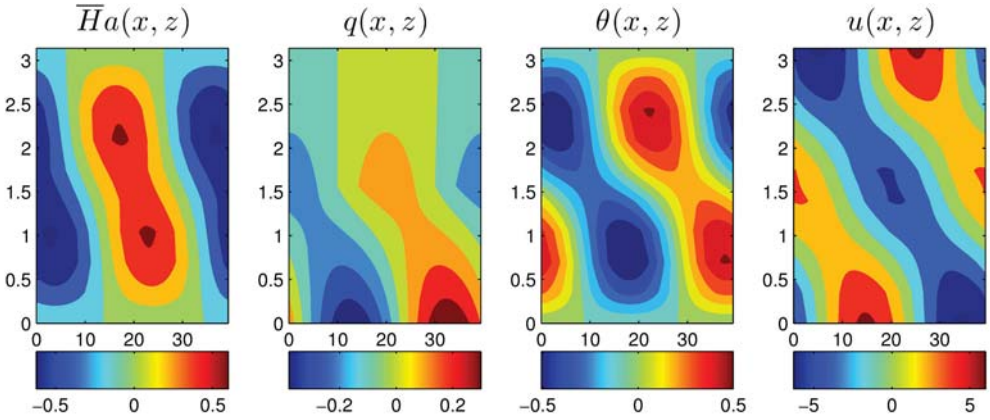

Figure 4: Skeleton model with three convective activities, structure $x - z$ of the MJO mode at the equator for $k = 1$. Contours of reconstructed heating $\overline{H}a$ (Kday^{-1}), moisture q (K), potential temperature θ (K) and zonal winds u (ms^{-1}), at the equator and as a function of x (1000 km) and z ($0 \le z \le \pi$ from the bottom to the tropopause).

another over a time step Δt read as follows:

$$\begin{aligned} &P\{\eta_d(t+\Delta t) = \eta_d(t) + 1\} = \lambda_d \Delta t + o(\Delta t) \\ &P\{\eta_d(t+\Delta t) = \eta_d(t) - 1\} = \mu_d \Delta t + o(\Delta t) \\ &P\{\eta_d(t+\Delta t) = \eta_d(t)\} = 1 - (\lambda_d + \mu_d)\Delta t + o(\Delta t) \\ &P\{\eta_d(t+\Delta t) \neq \eta_d(t) - 1,\ \eta_d(t),\ \eta_d(t) + 1\} = o(\Delta t)\,, \end{aligned} \tag{22}$$

where λ_d and μ_d are the upward and downward rates of transition, respectively (see TMS2014 for the deduction of their values from the amplitude equations). Similarly, we define $a_c = \Delta a \eta_c$ and $a_s = \Delta a \eta_s$ and compute suitable transition rates for those variables as well. The solving method for each stochastic skeleton model with refined vertical structure is similar to the one of TMS2014: we consider here a similar split-method between dry dynamics and convective processes, and a similar Gillespie algorithm for the stochastic processes

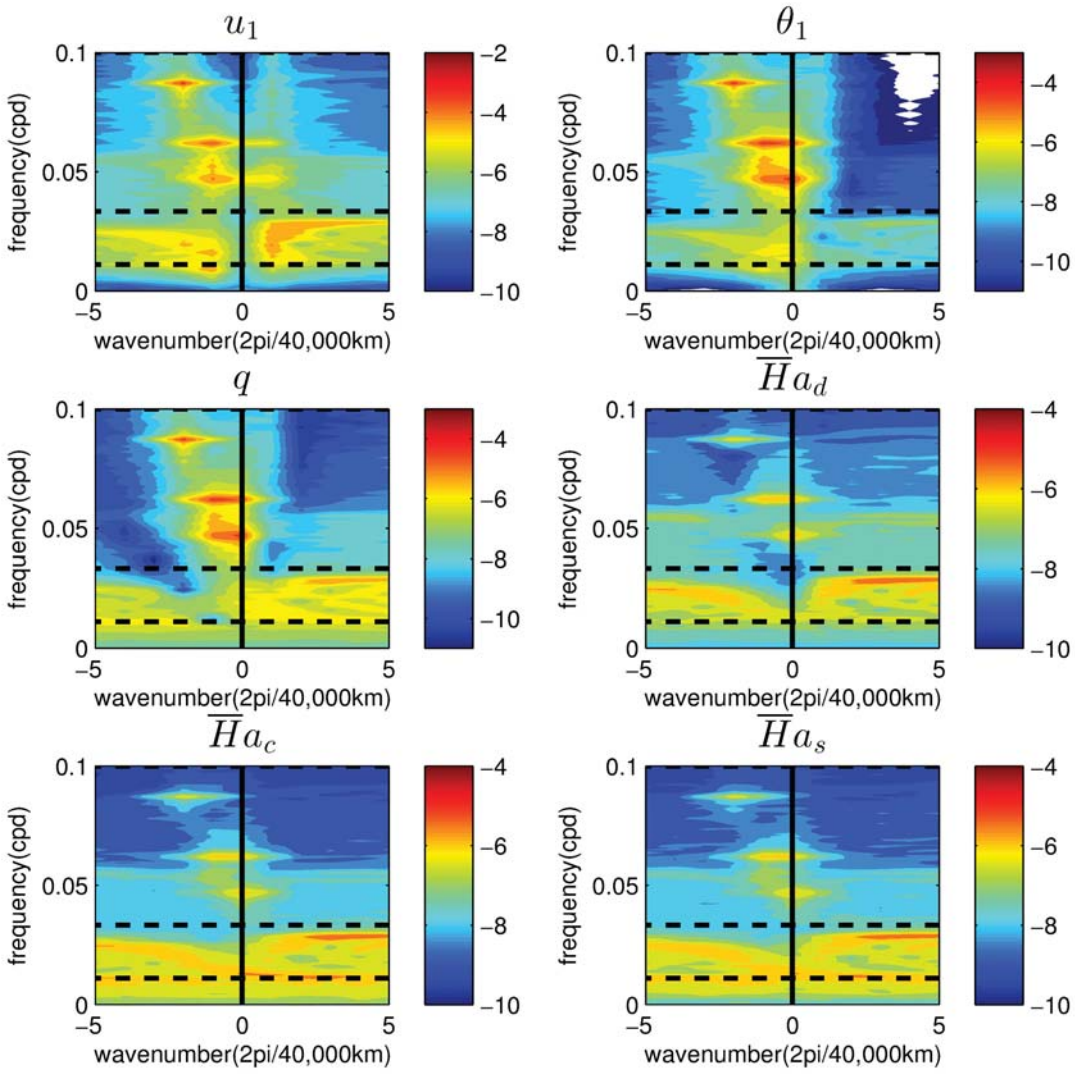

Figure 5: Skeleton model with three convective activities, zonal wavenumber-frequency power spectra: for u_1 (ms^{-1}), θ_1 (K), q (K), $\overline{H}a_d$, $\overline{H}a_c$ and $\overline{H}a_s$($Kday^{-1}$) taken at the equator, as a function of zonal wavenumber (in $2\pi/40000$ km) and frequency (cpd). The contour levels are in the base 10-logarithm, for the dimensional variables taken at the equator. The black dashed lines mark the periods 90 and 30 days.

of convective activities that is however extended to account for all transition rates (see [9], part III.B and III.C in particular).

We consider here an arbitrary yet plausible choice of parameter values for illustration of the solutions of each skeleton model. For all models, we consider the following parameter values identical to previous works (MS2009; TM2014; TM2015): $\overline{H} = 0.22$ $(10\,Kday^{-1})$, $\overline{Q} = 0.9$, $s_1^\theta = s^q = 0.22$ $(1\,Kday^{-1})$, $\Delta a = 0.001$, $\xi_{1d} = 1$, $\xi_{1c}, \xi_{1s} = 4/3\pi$, $\xi_{2c}, \xi_{2s} = 1/2$, $\overline{a}_c = \overline{a}_d = \overline{a}_s = s_1^\theta(\overline{H}(\xi_{1c} + \xi_{1d} + \xi_{1s}))^{-1}$, and $\epsilon_d = 0$, $\epsilon_c, \epsilon_s = 0.9$. Other parameters are slightly different for each model. For the skeleton model with three convective activities (sections 2.3 and 3), remaining parameters values are identical to TM2015: $(\Gamma_c\xi_{1c})$, $(\Gamma_d\xi_{1c})$, $(\Gamma_s\xi_{1s}) = 1$, $\beta_c(\xi_{1c}\xi_{1d})^{-1}, \beta_d(\xi_{1d}\xi_{1s})^{-1} = 1, \beta_s(\xi_{1s}\xi_{1c})^{-1} = 0.1$, in addition to $M = 0.02$ and $\alpha = 1$ for the secondary slaved circulation. Note that this peculiar expression of parameter values derives from the analysis of a rescaled model version in TM2015 where the dependency to ξ_{1d}, ξ_{1c} and ξ_{1s} is removed. For the skeleton model with coupling to potential temperature (sections 2.4 and 4), remaining parameters values are identical to the ones of the model with three convective activities, except for $\Gamma_d = 1.5$ and $(\Gamma_c\xi_{1c}) = 0.5$, in addition to $\lambda = 0.5$. For

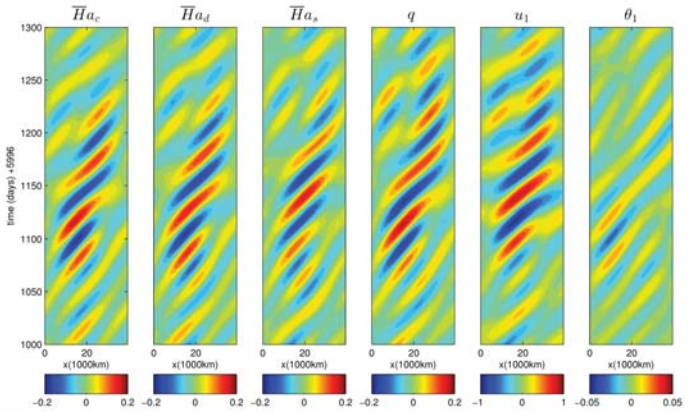

Figure 6: Skeleton model with three convective activities, hovmollers $x - t$: for $\overline{H}a_c$, $\overline{H}a_d$ and $\overline{H}a_s$ (Kday^{-1}), q (K), u_1 (ms^{-1}) and $\theta_1(K)$ at the equator and filtered in the MJO band (k=1-3, ω=1/30-1/70 cpd), as a function of zonal position (1000 km) and simulation time (days from reference time 5996 days).

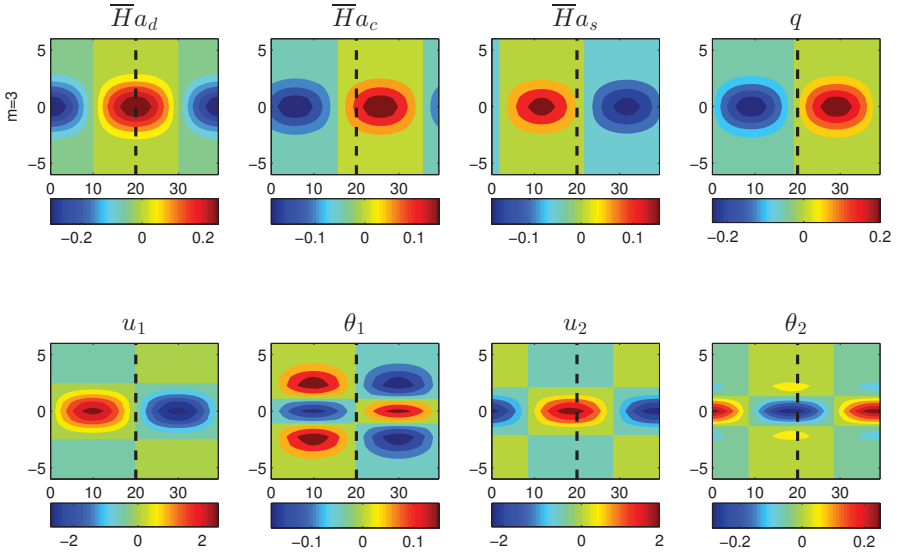

Figure 7: Skeleton model with coupled potential temperature, x-y Structure of the MJO mode for $k = 1$.See Fig. 3 for definitions.

the skeleton model with coupling to lower and middle level moisture (sections 2.5 and 4), remaining parameters values are identical to the ones of the model with three convective activities, except for $\Gamma_d, \Gamma_c, \Gamma_s = 1.5$, in addition to $\overline{Q}_1 = 0.9$, $\overline{Q}_2 = 0.7$, $\alpha_1 = 0.75$, $\alpha_2 = 0.25$. For the model with moisture flux presented in the appendix A, parameters are identical to the ones of TMS2014, with in addition $F_m = 0.005$ and $F_l = 0.03$. Finally, note that a meridional projection parameter $\gamma \approx 0.6$ in factor of the growth rates has been considered for each model in both linear solutions and the stochastic code (see TMS2014, its Eq. 4).

In the next sections, we will briefly present solutions for each of the above skeleton models with refined vertical structure. This includes an analysis of linear solutions with the above meridional truncation, in addition to an analysis of a numerical simulation with the above stochastic parametrization of convective activity. For each model the numerical simulation considers an idealized warm pool background state, as represented by the zonally varying external sources $s_1^\theta = s^q = 0.022(1 - 0.6\cos(2\pi x/L))$ at the equator (identical to TMS2014), where L is the equatorial belt length. We analyze the simulations output in the statistically equi-

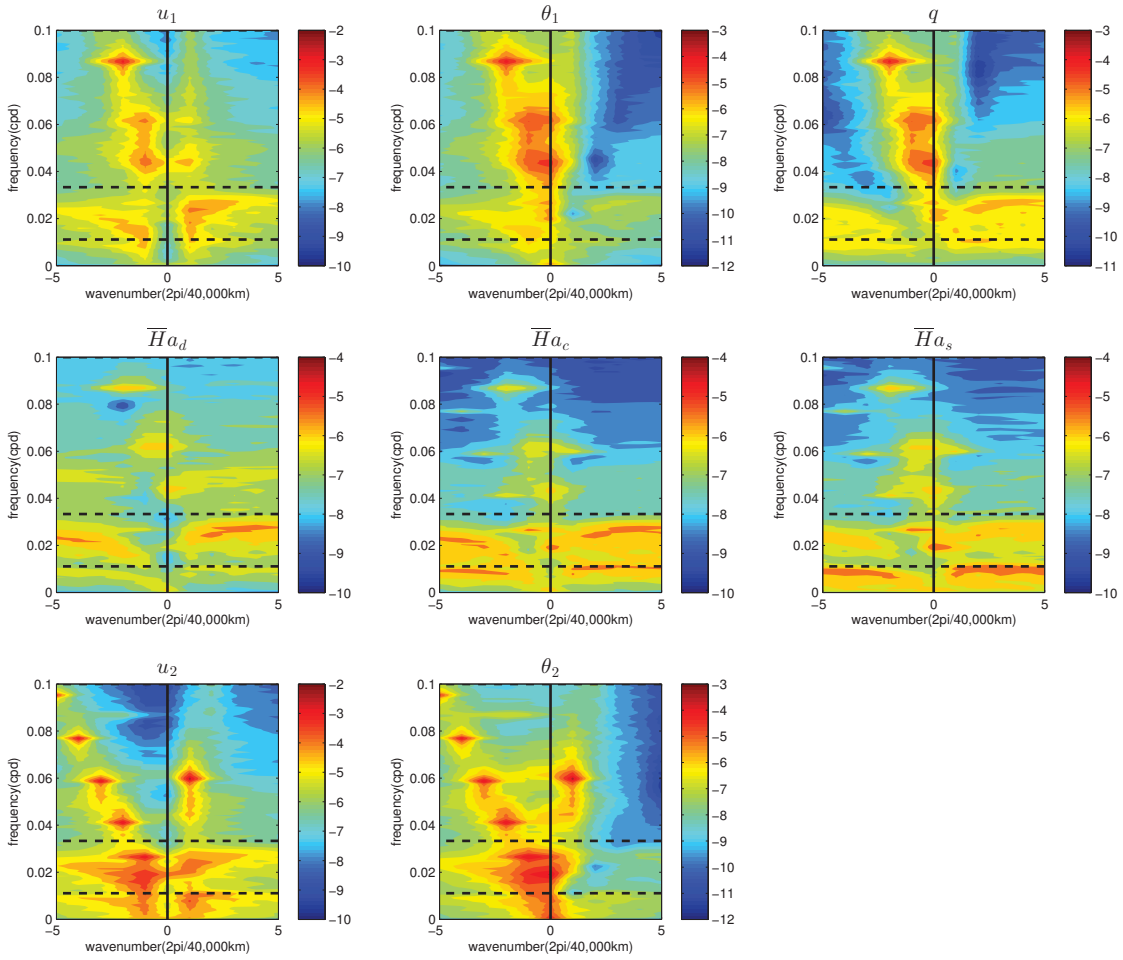

Figure 8: Skeleton model with coupled potential temperature, zonal wavenumber-frequency power spectra. See Fig. 5 for definitions.

librated regime. The reader is also invited to refer to previous work for further details on those diagnostics (MS2009; MS2011; TMS2014; TM2015).

3 Model with Three Convective Activities

In this section we present solutions for the model with three convective activities (see section 2.3). Most of these results have already been presented in TM2015, and are recalled here briefly for completeness. In addition to this, an analysis of a single-column version of the present model is provided in the appendix B. This analysis shows that the single-column version exhibits MJO-like oscillations that are irregular, intermittent and with similar frequency than the one of the MJO in the complete model.

The linear solutions of the present skeleton model with refined vertical structure are shown in Fig. 2. All linear solutions are neutral, as in the original skeleton model (MS2009). We consistently retrieve the original skeleton model solutions: a dry Kelvin ($\approx 55\ \mathrm{ms}^{-1}$), dry Rossby ($\approx -20\ \mathrm{ms}^{-1}$), MJO ($\approx 5\ \mathrm{ms}^{-1}$) and moist Rossby

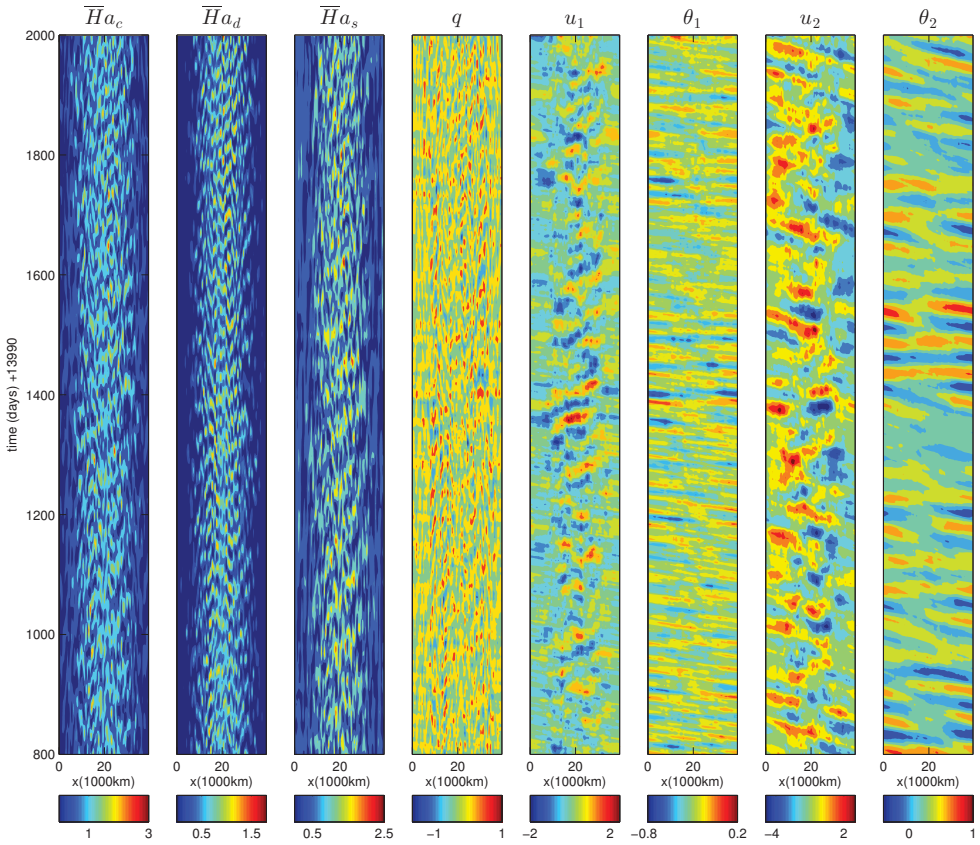

Figure 9: Skeleton model with coupled potential temperature, hovmollers $x - t$ at equator. See Fig. 6 for definitions.

(≈ -3 ms^{-1}) mode, for which the dispersion relationships are only slightly modified. There is in addition a slow eastward and a slow westward mode, with seasonal frequency (≤ 0.01 cpd).

Fig. 3 and 4 show the x-y structure and the equatorial x-z structure of the MJO mode, respectively, for a wavenumber $k = 1$. As in the original skeleton model, we retrieve moisture anomalies q leading deep convection a_d, as well as a quadrupole vortex structure on θ_1. In addition to this, the present model reproduces the front-to-rear structure of the MJO observed in nature on both heating, moisture, temperature and winds [19]. The front-to-rear structure is oriented westward/upward, with a progressive transition from congestus to deep to stratiform activity, a transition from lower to middle level moisture anomalies, and a transition from lower to upper wind anomalies and lower to upper temperature anomalies. Note that the phase lags between variables in Fig 3 (between a_c, a_d and a_s, between q_l and q_m, between θ_1 and θ_2 or between u_1 and u_2) give, by construction, the front-to-rear vertical structure in Fig 4. This is an attractive feature of the present skeleton model.

We show model solutions for a stochastic numerical simulation with a warm pool background (see section 2.7 for definitions). Note that for this numerical simulation the slaved secondary circulation (q_l, q_m, θ_2, u_2) is omitted as it is irrelevant to the main model dynamics. Fig. 5 shows the power spectra of the variables as a function of the zonal wavenumber k (in $2\pi/40,000$ km) and frequency ω (in cpd). The MJO appears here as a sharp power peak in the intraseasonal-planetary band ($1 \leq k \leq 5$ and $1/90 \leq \omega \leq 1/30$ cpd), most prominent in u_1, q, $\overline{H}a_d$ and also $\overline{H}a_c$ and $\overline{H}a_s$. Other noticeable features are the power peaks near the dispersion curves of the moist Rossby mode ($-5 \leq k \leq -1$, $\omega \approx 0.02$ cpd), slow eastward and slow westward

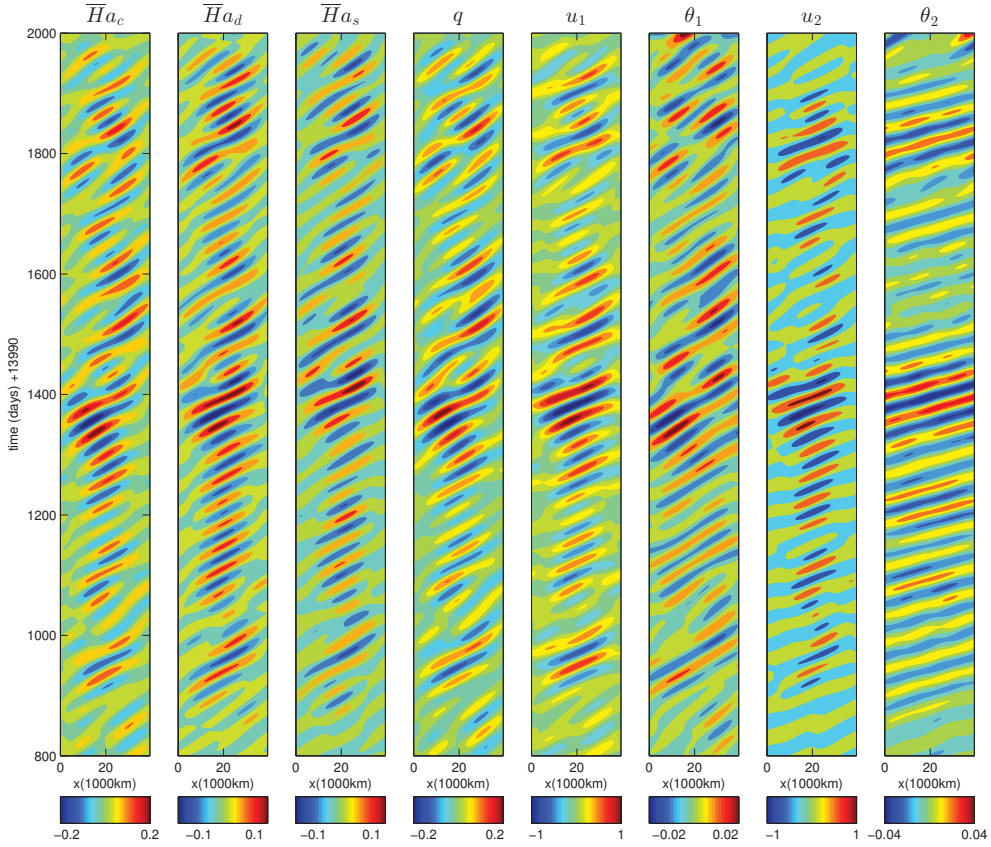

Figure 10: Skeleton model with coupled potential temperature, hovmollers $x-t$ at equator filtered in the MJO band (here k=1-3, w=1/30-1/70 cpd). hovmollers $x-t$ at equator. See Fig. 6 for definitions.

mode ($1 \leq k \leq 5$ or $-5 \leq k \leq -1$, $\omega \approx 0.01$ cpd, most prominent on $\overline{H}a_c$ and $\overline{H}a_s$). Finally, note that several synoptic scale features found in nature (e.g. convectively coupled Kelvin waves, etc) are here missing because the skeleton model dynamics are valid at the intraseasonal/planetary scale only.

Fig. 6 shows an example of Hovmoller diagrams filtered in the MJO band (k=1-3, ω =1/30-1/70 cpd). Note that the MJO band definition is slightly different than the one of previous works (TMS2014, where ω =1/30-1/90 cpd) in order to avoid grasping the seasonal variability associated to the slow modes. The MJO events are organized into irregular and intermittent wave trains with growth and demise, as seen in nature [29, 36], with a great diversity in strength, structure, lifetime and localization. There are in addition confined to the warm pool region (centered on $x = 20,000\,km$). The MJO events have structures in overall agreement with the MJO linear solution shown in Fig. 3: congestus activity $\overline{H}a_c$ and moisture q leads the deep convective activity center $\overline{H}a_d$, while stratiform activity $\overline{H}a_s$ trails behind, consistent with the MJO front-to-rear structure of convective activity found in nature [19].

4 Model with Coupled Potential Temperature

In this section we present the solutions of the model with coupled potential temperature (see section 2.4). In summary, like the model with three convective activities from previous section 3, this model reproduces a

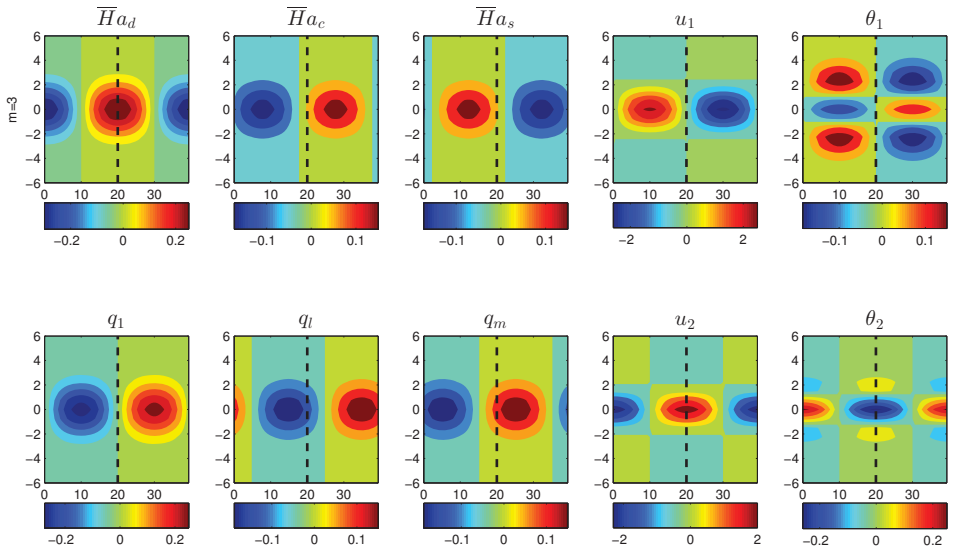

Figure 11: Skeleton model with coupled lower and middle tropospheric moisture, x-y Structure of the MJO mode for $k = 1$. See Fig. 3 for definitions.

MJO linear solution with a representative front-to-rear vertical structure, in addition to a representative and prominent intermittent MJO variability.

Fig. 7 shows the x-y structure of the MJO mode. Results are similar to the ones of previous section 3 (see Fig. 3), with a front-to-rear vertical structure on all variables, including heating, moisture, winds, and temperature. The dispersion relationships are also similar (see Fig. 2), except for an additional dry Kelvin 2 ($\approx 18\ ms^{-1}$) and dry Rossby 2 ($\approx -7\ ms^{-1}$) mode associated to the coupled dry dynamics of the second baroclinic mode $n = 2$ (not shown).

We show model solutions for a stochastic numerical simulation with a warm pool background. Fig. 8 shows power spectra for variables at equator. As in previous section 3, the MJO appears as a sharp power peak in the intraseasonal-planetary band. In comparison, congestus and stratiform activity have here a more prominent variability near the dispersion curves of the slow eastward and westward modes ($\omega \approx 0.01\ cpd$). In addition, the new variables u_2 and θ_2 show prominent power near the dispersion curves of the moist Rossby mode, dry Kelvin 2 and dry Rossby 2 modes. The dry Rossby 2 modes appear in figure 8 as straight lines starting from $\omega = 0$, $k = 0$ and reaching $\omega = 0.1$ cpd, $k = -5$. The dry Kelvin 2 with increased slope is harder to visualize but has a peak at $\omega = 0.06$ cpd, $k = 1$.

Fig. 9 shows an example of Hovmoller diagrams, and Fig. 10 shows the same Hovmoller diagrams filtered in the MJO band. The MJO variability is overall similar to the one in previous section 3 (see Fig. 6), organized into intermittent wave trains with growth and demise confined to the warm pool region. The new variables u_2, θ_2 show a consistent MJO variability when filtered in the MJO band, but show otherwise marked westward propagations in agreement with the power spectra in Fig. (8).

5 Model with Coupled Lower and Middle Tropospheric Moisture

In this section we present the solutions of the model with coupled lower and middle tropospheric moisture (see section 2.5). In summary, like the model with three convective activities from previous section 3, this model reproduces a MJO linear solution with a representative front-to-rear vertical structure, in addition to a representative intermittent MJO variability. However, the MJO variability is here less prominent in compari-

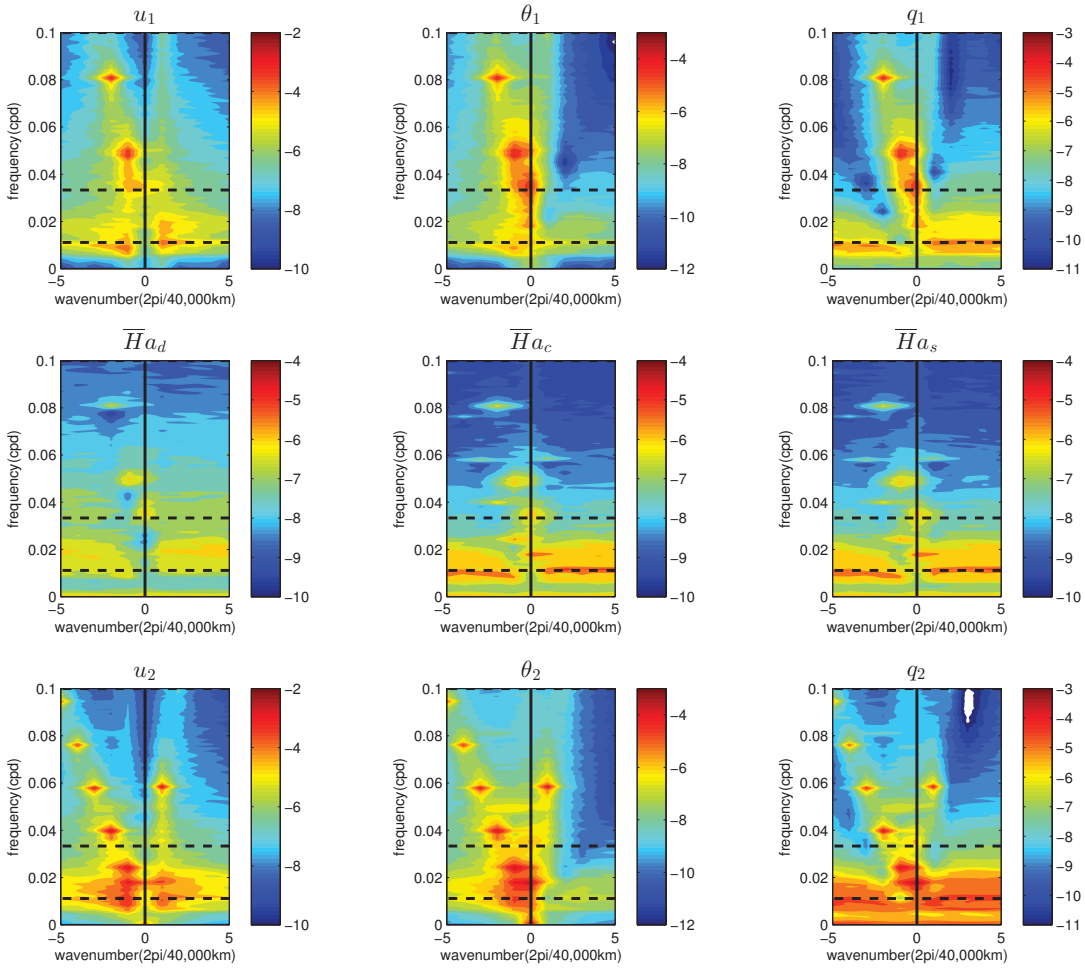

Figure 12: Skeleton model with coupled lower and middle tropospheric moisture, zonal wavenumber-frequency power spectra. See Fig. 5 for definitions.

son, which is likely due to the prominent variability associated to additional linear solutions (slow eastward and westward modes, zonally symmetric mode).

Fig. 11 shows the x-y structure of the MJO mode. Results are similar to the ones of previous section 3 (see Fig. 3). The dispersion relationships are also similar (see Fig. 2), except for an additional dry Kelvin 2 ($\approx 18\, ms^{-1}$) and dry Rossby 2 ($\approx -7\, ms^{-1}$) mode associated to the second baroclinic mode $n = 2$ and a zonally symmetric mode for which $\omega = 0$ and $a_d, a_c, a_d, q_2 \neq 0$ (not shown).

We show model solutions for a stochastic numerical simulation with a warm pool background. Fig. 12 shows power spectra for variables at equator. As in previous section 3, the MJO appears here as a power peak in the intraseasonal-planetary band, but is here less pronounced especially on the convective activities a_d, a_c and a_s. For instance congestus and stratiform activity have a most prominent variability near the dispersion curves of the slow eastward and westward modes ($\approx 0.01\, cpd$). Another new feature is the power peak near the dispersion curve of the zonally symmetric mode ($\omega = 0$) as seen on variables a_d, a_c, a_s and q_2. In addition, the new variables u_2, θ_2 and q_2 show prominent power near the dispersion curves of the moist Rossby mode, dry Kelvin 2 and dry Rossby 2 modes.

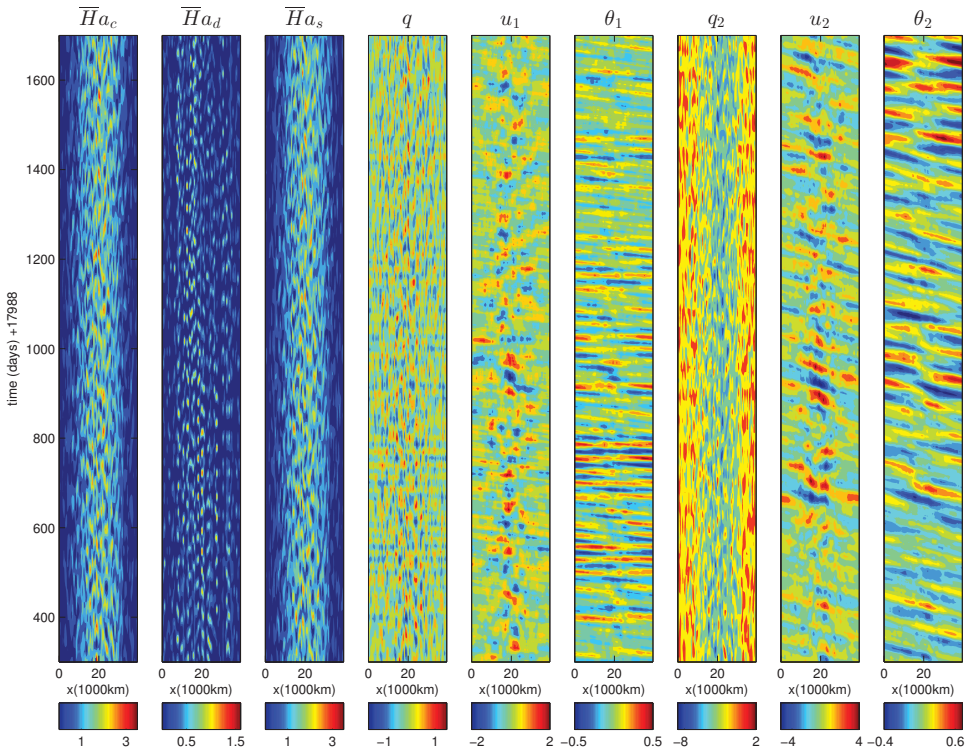

Figure 13: Skeleton model with coupled lower and middle tropospheric moisture, hovmollers $x - t$ at equator. See Fig. 6 for definitions.

Fig. 13 shows an example of Hovmoller diagrams, and Fig. 14 shows the same Hovmoller diagrams filtered in the MJO band. The MJO variability is overall similar to the one in previous section 3 (see Fig. 6), organized into intermittent wave trains with growth and demise confined to the warm pool region. The MJO events in Fig. (14) have however a weaker amplitude of deep activity a_d, which is likely due to the marked standing components on this variable in Fig. (13). The new variables u_2, θ_2 and q_2 show a consistent MJO variability when filtered in the MJO band, but show otherwise marked westward propagations for u_2 and θ_2 and standing components for q_2, in agreement with the power spectras in Fig. (12).

6 Discussion

We have proposed and analyzed a suite of skeleton models that qualitatively reproduce the refined vertical structure of the MJO in nature. The present models have all been designed following similar guiding principles such as the conservation of a positive energy and a moist static energy. The solutions of each model have been analyzed. All models reproduces qualitatively the front-to-rear (i.e. tilted) vertical structure of the MJO found in nature, with MJO events marked by a planetary envelope of convective activity transitioning from the congestus to the deep to the stratiform type, in addition to a front-to-rear structure of heating, moisture, winds and temperature. When considered with a simple stochastic parametrization for the unresolved details of synoptic-scale activity, all models show intermittent initiation, propagation and shut down of MJO wave trains, as in previous studies.

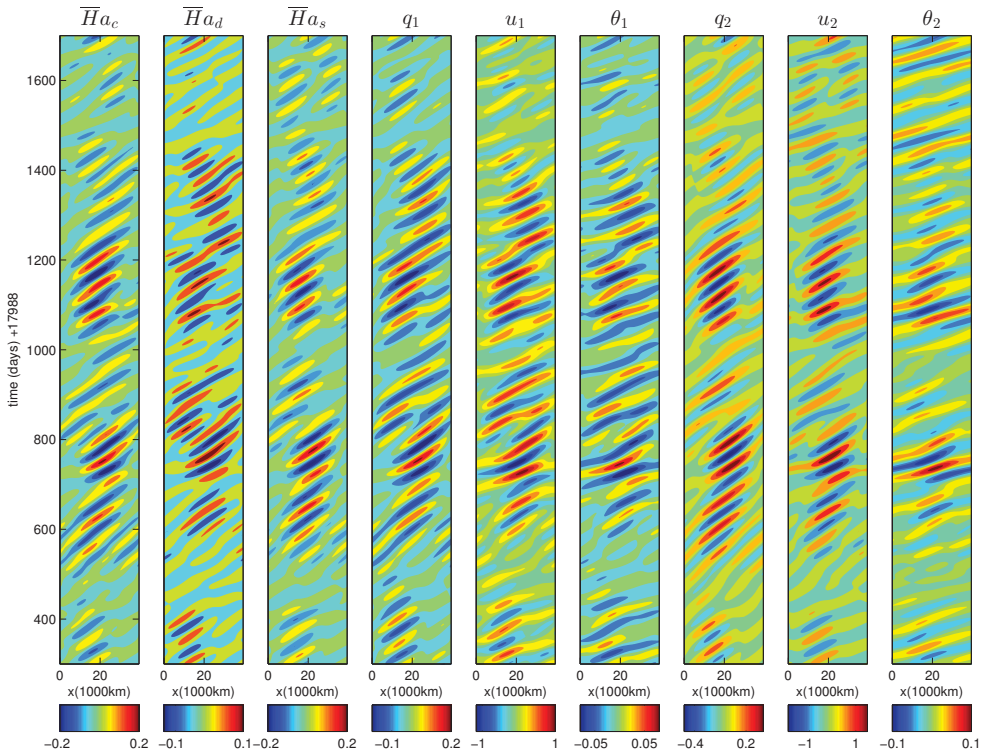

Figure 14: Skeleton model with coupled lower and middle tropospheric moisture, hovmollers $x - t$ at equator filtered in the MJO band (here k=1-3, w=1/30-1/70 cpd). See Fig. 6 for definitions.

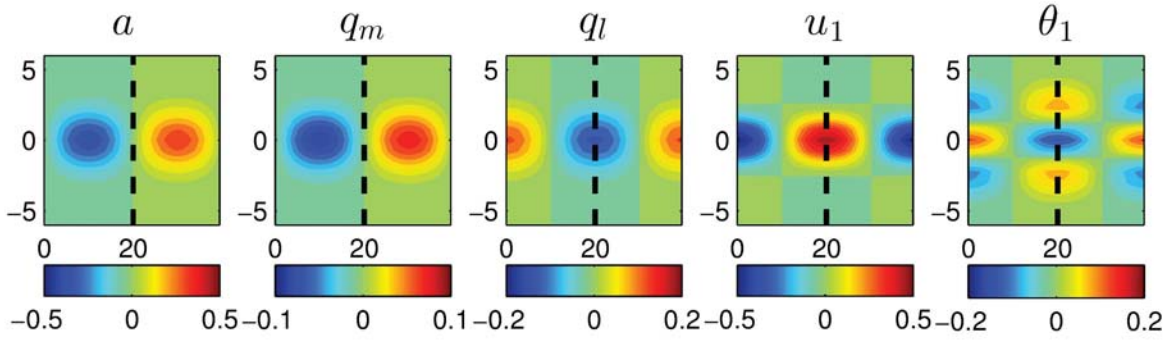

Figure 15: Skeleton model with moisture flux, x-y Structure of the MJO mode for $k = 1$. See Fig. 3 for definitions.

A general question that is addressed in the present article is to which extent the skeleton model can be complexified towards more realism. As compared to the original skeleton model from Majda and Stechmann [27], the models proposed here have richer dynamics and include more details of the vertical structure of the MJO . The new classes of skeleton models all have their own strengths and weaknesses, as already discussed in section 2.6. The models strongly differ with respect to the separation of the dynamics into a coupled circulation and a secondary slaved circulation. In particular, the new models with coupled potential temperature (section 2.5 and 4) or with coupled lower and middle level moistures (section 2.5 and 5) are fully coupled i.e. have no secondary slaved circulation, which is more realistic. A drawback of this higher dimensionality is the introduction in those models of several additional linear solutions (e.g. a slow eastward and westward

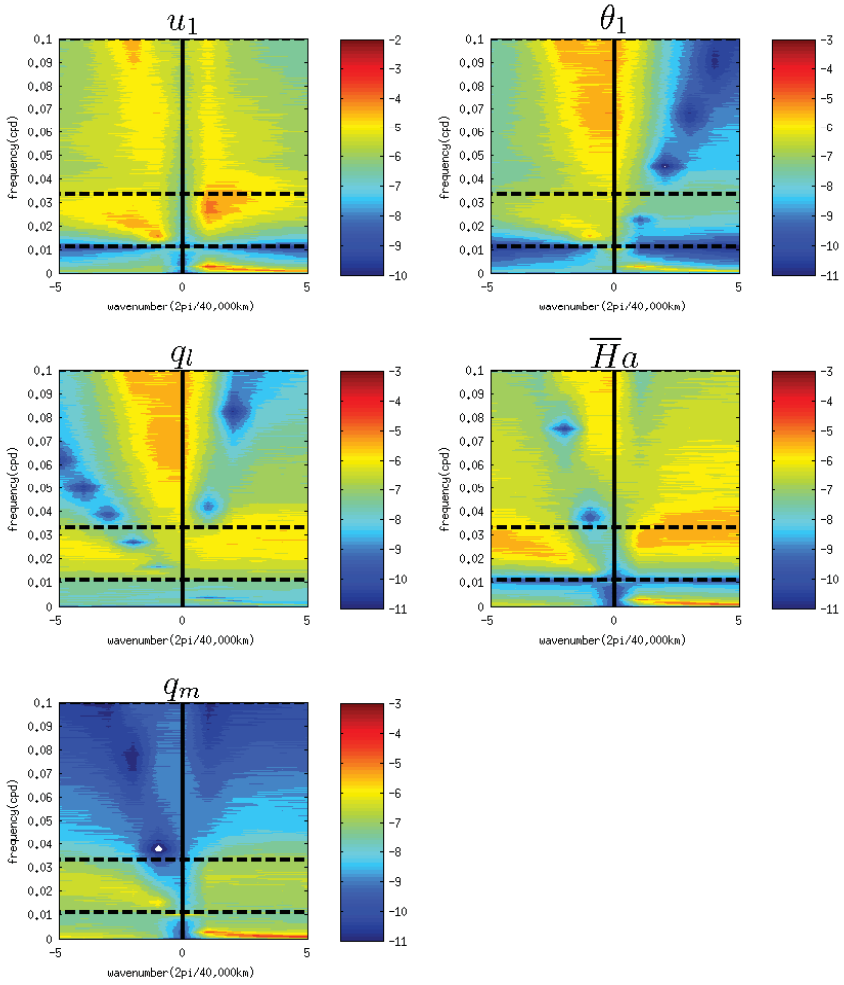

Figure 16: Skeleton model with moisture flux, zonal wavenumber-frequency power spectra. See Fig. 5 for definitions.

mode, a zonally symmetric mode, etc). For instance, those additional linear solutions can be as prominent as the MJO variability in numerical simulations. Nevertheless those additional linear solutions are usually of a seasonal or interannual frequency, and are therefore separable from the intraseasonal MJO variability. Suitable regimes where this feature is avoided could also be found for different parameter values [5]. Note that a general assumption in the original skeleton model [27] and the present models is that the MJO arises from neutrally-stable interactions at the planetary scale, while main instabilities occur on the synoptic scale. This view differs from the one of a MJO planetary instability [45], and is also the reason why additional linear solutions (also neutrally-stable) must be treated carefully as they may be as prominent as the MJO variability. For future work, additional classes of skeleton models that respect this assumption may be constructed starting from the energy conservation principle of the present article.

While the present skeleton models appear to be plausible representations for the essential mechanisms of the MJO, several issues need to be addressed as a perspective for future work. First, although we have illustrated here the model solutions for an arbitrary yet plausible choice of parameters, there are many other interesting parameter regimes that should be analyzed. Another important issue is to compare further the models solutions with their observational surrogates, qualitatively and also quantitatively. For instance, the

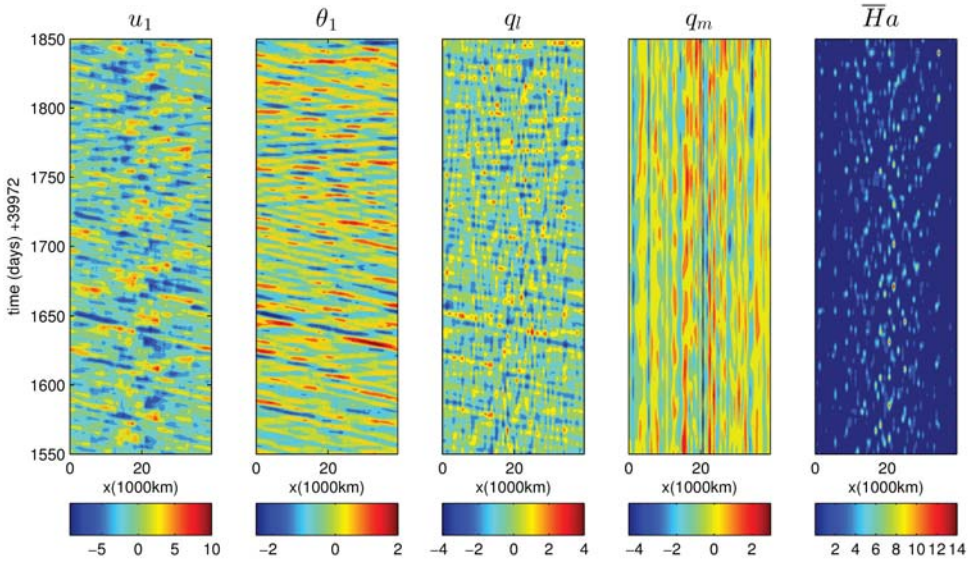

Figure 17: Skeleton model with moisture flux, hovmollers $x - t$ at equator. See Fig. 6 for definitions.

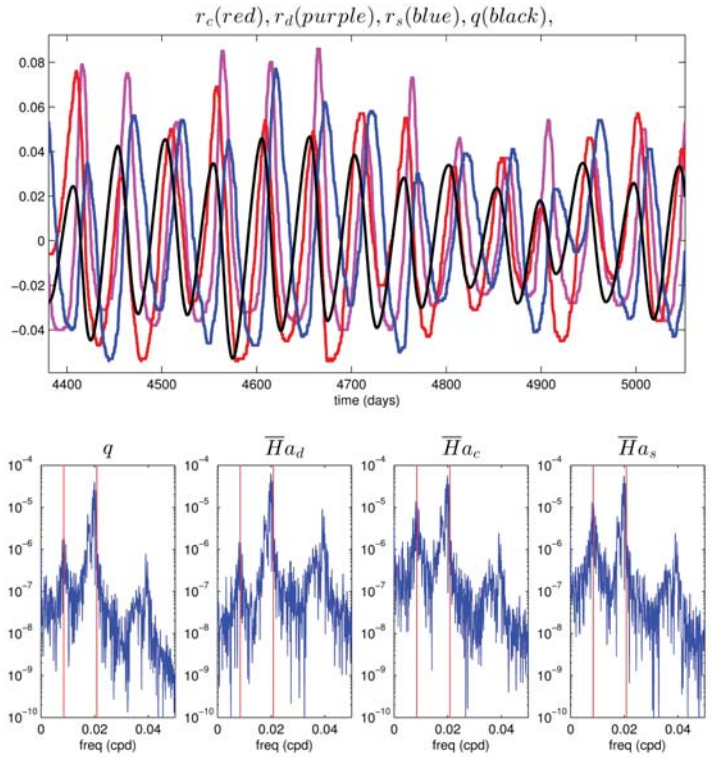

Figure 18: Skeleton model with three convective activities, single-column version. Top: timeseries of r_c(red), r_d (purple), r_s (blue), q (black), as a function of time (days). Bottom: power spectra, as a function of frequency (cpd). The red lines mark the frequencies of linear solutions: SC-slow mode ($\approx 0.008\ cpd$) and SC-MJO mode (≈ 0.02 cpd). .

solutions could be analyzed for a more realistic background of heating/moisture [34] and/or for more realistic parameters deduced from observations (e.g. [5, 12]). In addition, the present models could be used to analyze zonal variations of the characteristics of the MJO front-to-rear structure [19] or to provide new theoretical

estimates of MJO events in observations [38]. More complete models should also account for more detailed sub-planetary processes within the envelope of intraseasonal events, including for example synoptic-scale convectively coupled waves and/or mesoscale convective systems (e.g. [7, 12, 25, 31]).

Acknowledgement: The research of A.J.M. is partially supported by the Office of Naval Research Grant ONR MURI N00014 -12-1-0912. S.T. is supported as a postdoctoral fellow through A.J.M's ONR MURI Grant.

Appendix A: Model with Moisture Flux

In this appendix section, we briefly present numerical solutions for the skeleton model with moisture flux used in section 2.2. This model reproduces a MJO linear solution with a representative front-to-rear vertical structure, in addition to a representative and prominent intermittent MJO variability.

Fig. 15 shows the structure of the MJO mode: it is similar to the one of the original skeleton model (MS2009), with in addition middle level moisture q_m trailing behind lower level moisture q_l, resulting in a tilted vertical structure of moisture by construction. The dispersion relationships of the present model are identical to the ones of the original skeleton model, with in addition a slow eastward mode propagating at around $0.5\ ms^{-1}$(not shown).

We show model solutions for a stochastic numerical simulation with a warm pool background (see section 2.7 for definitions). Fig. 16 shows power spectra for variables at equator. The power spectra are similar to the ones of the stochastic skeleton model from TMS2014, with the MJO appearing as a sharp power peak in the intraseasonal-planetary band ($1 \le k \le 5$ and $1/90 \le \omega \le 1/30$ cpd). The additional variable q_m shows a sharp power peak near the dispersion curve of the moist Rossby mode ($-5 \le k \le -1$, $\omega \approx 0.02$ cpd) and the slow eastward mode ($1 \le k \le 5$, $\omega \approx 0$ cpd). Fig. 17 shows an example of Hovmoller diagrams. Some propagations of MJO events are visible (e.g. on u_1, a). The middle level moisture q_m is marked by near prominent standing components and some westward propagations, consistent with the power spectra from Fig (16).

Appendix B: Model with Three Convective Activities, Single-Column Version

We analyze here a single-column version of the skeleton model with three convective activites (see sections 2.3 and 3). With a stochastic parametrization of convective activity (TMS2014; TM2015), this model produces intraseasonal oscillations with a progression from congestus to deep then stratiform activity, that are simple surrogates of the MJO vertical structure in the complete model.

The single-column model version is here obtained assuming the weak temperature approximation in Eq. (8) (see appendix of [28, 35]). The single-column version reads,

$$\begin{aligned}
\partial_t q &= -(1-\overline{Q})\overline{H}(\xi_{1d}a_d + \xi_{1c}a_c + \xi_{1s}a_s) + (\overline{Q}s_1^\theta - s^q)\\
\partial_t a_c &= \Gamma_c(\xi_{1c}q + \beta_s r_s - \beta_c r_d)(a_c - \epsilon_c r_c)\\
\partial_t a_d &= \Gamma_d(\xi_{1d}q + \beta_c r_c - \beta_d r_s)(a_d - \epsilon_d r_d)\\
\partial_t a_s &= \Gamma_s(\xi_{1s}q + \beta_d r_d - \beta_s r_c)(a_s - \epsilon_s r_s)\,.
\end{aligned} \tag{23}$$

We first consider the linear solutions of this system, that consist of two oscillating eigenmodes (not shown). First, the SC-MJO mode (for single-column MJO mode) has the characteristics of the MJO and moist Rossby modes in the complete model: its frequency is similar (≈ 0.02 cpd) and it shows a progression from congestus to deep then stratiform activity. Note that a similar result is found for the original skeleton model, which single-column version exhibits a similar frequency [28]. The SC-slow mode has the characteristics of the slow eastward and slow westward modes in the complete model: its frequency is similar ($\approx$ 0.008 cpd) and it shows an opposite progression from stratiform to deep to congestus activity. This counterintuitive behaviour

is due to the transition rates terms (β_c, β_d, β_s) in the model that may allow for unrealistic progressions of convective activity (see TM2015). The SC-slow mode is however less prominent in numerical simulations, as shown below.

We now consider solutions of this system with a stochastic parametrization of convective activity (see section 2.7, TM2015). Fig. 18 shows timeseries for an example of numerical simulation (with parameters as in section 2.7 and random initial conditions). There are intraseasonal oscillations of varying strength and intensity with a progression from congestus to deep to stratiform activity, similar to the structure of the SC-MJO mode. This is consistent with the power spectra also shown in Fig. 18 where power peaks on all variables at the SC-MJO mode frequency (≈ 0.02 cpd). In Fig. 18, there are also peaks on each variable near the frequency of the SC-slow mode (≈ 0.008 cpd). There is also a third peak at twice the frequency of the SC-MJO mode (≈ 0.04 cpd), that is likely due to simple nonlinear interactions (see e.g. figure 2 of [41] for similar results).

References

[1] S. Ajayamohan, B. Khouider, and Andrew J. Majda. Realistic initiation and dynamics of the Madden-Julian Oscillation in a coarse resolution aquaplanet GCM. *Geophys. Res. Lett.*, 40:6252–6257, 2013.

[2] Joseph A. Biello and Andrew J. Majda. A New Multiscale Model for the Madden-Julian Oscillation. *J. Atmos. Sci.*, 62(6):1694–1721, 2005.

[3] Joseph A. Biello and Andrew J. Majda. Modulating synoptic scale convective activity and boundary layer dissipation in the IPESD models of the Madden-Julian oscillation. *Dyn. Atm. Oceans*, 42, Issue 1-4:152–215, 2006.

[4] N. Chen and A. J. Majda. Filtering the Stochastic Skeleton Model for the Madden-Julian Oscillation. 2015. in press.

[5] N. Chen, A. J. Majda, and D. Giannakis. Predicting the cloud patterns of the madden-julian oscillation through a low-order nonlinear stochastic model. *GRL*, page DOI: 10.1002/2014GL060876, 2014.

[6] Q. Deng, B. Khouider, and A. J. Majda. The MJO in a Coarse-Resolution GCM with a Stochastic Multicloud Parameterization. *J. Atmos. Sci.*, 72, 2015. 55-74.

[7] Yevgeniy Frenkel, Andrew J. Majda, and Boualem Khouider. Using the Stochastic Multicloud Model to Improve Tropical Convective Parameterization: A Paradigm Example. *J. Atmos. Sci.*, 69:1080–1105, 2012.

[8] C. W. Gardiner. *Handbook of stochastic methods for physics, chemistry, and the natural sciences*. Springer, 1994. 442pp.

[9] Daniel T. Gillespie. Exact Stochastic Simulation of Coupled Chemical Reactions. *J. Phys. Chem.*, 81(25):2340–2361, 1977.

[10] Harry H. Hendon and Murry L. Salby. The Life Cycle of the Madden-Julian Oscillation. *J. Atmos. Sci.*, 51:2225–2237, 1994.

[11] X. Jiang, D. E. Waliser, and coauthors. Vertical structure and physical processes of the Madden-Julian oscillation: Exploring key model physics in climate simulations. *J. Geophys. Res.*, 2015. doi:10.1002/2014JD022375.

[12] B. Khouider, J. A. Biello, and A. J. Majda. A Stochastic Multicloud Model for Tropical Convection. *Comm. Math. Sci.*, 8(1):187–216, 2010.

[13] B. Khouider and A. J. Majda. A simple multicloud parametrization for convectively coupled tropical waves. Part I: Linear Analysis. *J. Atmos. Sci.*, 63:1308–1323, 2006.

[14] B. Khouider and A. J. Majda. A simple multicloud parametrization for convectively coupled tropical waves. Part II. Nonlinear simulations. *J Atmos Sci*, 64:381–400, 2007.

[15] B. Khouider and A. J. Majda. Equatorial convectively coupled waves in a simple multicloud model. *J Atm Sci*, (65):3376–3397, 2008.

[16] Boualem Khouider and Andrew J. Majda. Multicloud Models for Organized Tropical Convection: Enhanced Congestus Heating. *J. Atmos. Sci.*, 65(3):895–914, 2008.

[17] Boualem Khouider, Amik St-Cyr, Andrew J. Majda, and Joseph Tribbia. The MJO and convectively coupled waves in a coarse-resolution GCM with a simple multicloud parameterization. *J. Atmos. Sci.*, 68(2):240–264, 2011.

[18] K. Kikuchi and Y. N. Takayabu. The development of organized convection associated with the MJO during TOGA COARE IOP: Trimodal characteristics. *Geophys. Res. Lett.*, 31, 2004. L10101,doi:10.1029/2004GL019601.

[19] G. N. Kiladis, K. H. Straub, and Haertel P. T. Zonal and vertical structure of the Madden-Julian oscillation. *J Atmos Sci*, 62:2790–2809, 2005.

[20] N.P. Klingaman, X. Jiang, and coauthors. Vertical structure and physical processes of the Madden-Julian oscillation: Synthesis and summary. *J. Geophys. Res.*, 2015. doi:10.1002/2015JD023196.

[21] Gregory F. Lawler. *Introduction to Stochastic Processes*. Chapman and Hall/CRC, 2006. 192pp.

[22] R. E. Madden and P. R. Julian. Detection of a 40-50 day oscillation in the zonal wind in the tropical Pacific. *J. Atmos. Sci.*, 28:702–708, 1971.

[23] R. E. Madden and P. R. Julian. Observations of the 40-50 day tropical oscillation-A review. *Mon. Wea. Rev.*, 122:814–837, 1994.

[24] A. J. Majda and J. A. Biello. A multiscale model for tropical intraseasonal oscillations. *Proc. Natl. Acad. Sci. USA*, 101:4736–4741, 2004.
[25] A. J. Majda, S. N. Stechmann, and B. Khouider. Madden-Julian oscillation analog and intraseasonal variability in a multicloud model above the equator. *Proc. Natl. Acad. Sci. USA*, 104:9919–9924, 2007.
[26] Andrew J. Majda and Samuel N. Stechmann. A Simple Dynamical Model with Features of Convective Momentum Transport. *J. Atmos. Sci.*, 66:373–392, 2009.
[27] Andrew J. Majda and Samuel N. Stechmann. The skeleton of tropical intraseasonal oscillations. *Proc. Natl. Acad. Sci.*, 106:8417–8422, 2009.
[28] Andrew J. Majda and Samuel N. Stechmann. Nonlinear Dynamics and Regional Variations in the MJO Skeleton. *J. Atmos. Sci.*, 68:3053–3071, 2011.
[29] A. J. Matthews. Primary and successive events in the Madden-Julian Oscillation. *Quart. J. Roy. Meteor. Soc.*, 134:439–453, 2008.
[30] T. Miyakawa, Y.N. Takayabu, T. Nasuno, H. Miura, M. Satoh, and M.W. Moncrieff. Convective momentum transport by rain-bands within a Madden-Julian oscillation in a global nonhydrostatic model with explicit deep convective processes. Part I: Methodology and general results. *J. Atmos. Sci.*, 69:1317–1338, 2012.
[31] M. W. Moncrieff, M. Shapiro, J. Slingo, and F. Molteni. Collaborative research at the intersection of weather and climate. *WMO Bull.*, 56:204–211, 2007.
[32] MW Moncrieff. Analytic representation of the large-scale organization of tropical convection. *Quart. J. Roy. Meteor. Soc.*, 130:1521–1538, 2004.
[33] J. D. Neelin and N. Zeng. A quasi-equilibrium tropical circulation model:formulation. *J. Atmos. Sci.*, 57:1741–1766, 2000.
[34] H. R. Ogrosky and S. N. Stechmann. The mjo skeleton model with observation-based background state and forcing. *Q. J. Roy. Met. Soc.*, 2015. DOI: 10.1002/qj.2552.
[35] A. H. Sobel, J. Nilsson, and L. M. Polvani. The Weak Temperature Gradient Approximation and Balanced Tropical Moisture Waves. *J. Atmos. Sci.*, 58:3650–3665, 2001.
[36] J. P. Stachnik, D. E. Waliser, and A.J. Majda. Precursor environmental conditions associated with the termination of madden-julian oscillation events. *J. Atmos. Sci.*, 2015. doi: http://dx.doi.org/10.1175/JAS-D-14-0254.1.
[37] S. Stechmann, A. J. Majda, and D. Skjorshammer. Convectively coupled wave-environment interactions. *Theor. Comp. Fluid Dyn.*, 27:513–532, 2013.
[38] S. N. Stechmann and A. J. Majda. Identifying the skeleton of the madden-julian oscillation in observational data. *Mon. Wea. Rev.*, 143:395–416, 2015.
[39] S. Thual and A. J. Majda. A skeleton model for the MJO with refined vertial structure. *Clim. Dyn.*, 2015. accepted.
[40] S. Thual, A.-J. Majda, and S. N. Stechmann. Asymmetric intraseasonal events in the skeleton MJO model with seasonal cycle. *Clim. Dyn.*, 2015. doi:10.1007/s00382-014-2256-8.
[41] S. Thual, Andrew J. Majda, and S. N. Stechmann. A stochastic skeleton model for the MJO. *J. Atmos. Sci.*, 71:697–715, 2014.
[42] B. Tian, D. Waliser, E. Fetzer, B. Lambrigsten, Y. Yung, and B. Wang. Vertical moist thermodynamic structure and spatial-temporal evolution of the MJO in AIRS observations. *J. Atmos. Sci.*, 63:2462–2485, 2006.
[43] Matthew Wheeler and George N. Kiladis. Convectively Coupled Equatorial Waves: Analysis of Clouds and Temperature in the Wavenumber-Frequency Domain. *J. Atmos. Sci.*, 56:374–399, 1999.
[44] P. K. Xavier, J. C. Petch, and coauthors. Vertical structure and physical processes of the Madden-Julian Oscillation: Biases and uncertainties at short range. *J. Geophys. Res.*, 2015. doi:10.1002/2014JD022718.
[45] Chidong Zhang. Madden-Julian Oscillation. *Rev. Geophys.*, 43, 2005. RG2003, doi:10.1029/2004RG000158.